

# Design, Optimise and Evaluate a Power Management System for Harvesting Nano-energy.

By

Tanisha Rose Soldini

Engineering (Robotics) (Honours) / Master of Engineering  
(Electronics)

*Thesis*

*Submitted to Flinders University for the degree of*

**Bachelor of Engineering (Robotics) (Honours) /**

**Master of Engineering (Electronics)**

College of Science and Engineering

18/04/2024

---

# TABLE OF CONTENTS

<b>EXECUTIVE SUMMARY.....</b>	<b>5</b>
<b>DECLARATION .....</b>	<b>6</b>
<b>ACKNOWLEDGEMENTS.....</b>	<b>7</b>
<b>LIST OF FIGURES.....</b>	<b>8</b>
<b>LIST OF TABLES .....</b>	<b>10</b>
<b>INTRODUCTION.....</b>	<b>11</b>
<b>Background.....</b>	<b>11</b>
<b>Current Solutions .....</b>	<b>11</b>
<b>Triboelectric Nanogenerator (TENG) .....</b>	<b>12</b>
<b>Objectives.....</b>	<b>12</b>
<b>Project Scope.....</b>	<b>12</b>
<b>Outline .....</b>	<b>13</b>
<b>LITERATURE REVIEW.....</b>	<b>14</b>
<b>1. Triboelectric Nanogenerator (TENG) Mechanism.....</b>	<b>14</b>
<b>2. Current solutions through optimisation of TENG materials and structures.....</b>	<b>15</b>
<b>3. Recent progress of power management system adopted in TENG.....</b>	<b>18</b>
3.1. TENG Charge Boosting.....	18
3.2. AC to DC Conversions .....	21
3.3. Impedance Matching.....	22
3.4. Voltage Regulation .....	23
<b>4. Comparison .....</b>	<b>25</b>
<b>5. Conclusion .....</b>	<b>25</b>
<b>METHODOLOGY.....</b>	<b>27</b>
<b>General Process .....</b>	<b>27</b>
<b>Assumptions and Constraints .....</b>	<b>27</b>
<b>Triboelectric Nanogenerator (TENG) Device .....</b>	<b>28</b>
<b>Charge Pumping Method .....</b>	<b>28</b>
Voltage Multiplier Circuit.....	29

<b>LTC3588 Energy Harvester Chip .....</b>	<b>30</b>
<b>Power Management System .....</b>	<b>31</b>
<b>Equipment and Setup.....</b>	<b>32</b>
<b>Evaluation Procedure.....</b>	<b>33</b>
E1. TENG .....	34
E2. Voltage Multiplier Circuit .....	34
E3. LTC3588 Energy Harvester Chip.....	34
E4. Power Management System.....	34
<b>Processing Data.....</b>	<b>35</b>
<b>Experimental Errors .....</b>	<b>35</b>
<b><i>RESULTS</i>.....</b>	<b>36</b>
<b>Results.....</b>	<b>36</b>
Voltage Recordings.....	36
Current Recordings.....	38
Power Recordings.....	38
Visual Representation.....	39
<b>Statistical Analysis.....</b>	<b>40</b>
<b>Discussion .....</b>	<b>42</b>
<b><i>CONCLUSION</i> .....</b>	<b>45</b>
<b><i>FUTURE WORK</i>.....</b>	<b>46</b>
<b><i>REFERENCES</i>.....</b>	<b>47</b>
<b><i>APPENDICES</i> .....</b>	<b>54</b>
<b>Appendix A: Equipment Specifications.....</b>	<b>54</b>
<b>Appendix B. TENG Configuration .....</b>	<b>56</b>
<b>Appendix C. Voltage Multiplier Circuit Configuration.....</b>	<b>56</b>
<b>Appendix D. LTC3588 Energy Harvester Chip Configuration .....</b>	<b>57</b>
<b>Appendix E. Power Management System Configuration .....</b>	<b>57</b>
<b>Appendix F. Power Management System Circuit Design .....</b>	<b>58</b>
<b>Appendix G. Python Code.....</b>	<b>59</b>
<b>Appendix H. Python Code for Statistical Analysis.....</b>	<b>65</b>

Voltage Data from Power Management System.....	65
Current Data from Power Management System.....	67

## **EXECUTIVE SUMMARY**

This study investigates the design, optimisation, and evaluation of a power management system (PMS) for harvesting nano-energy, specifically focusing on triboelectric nanogenerators (TENG). The overall objective is to create a self-sufficient power source that can extract electrical energy from low-frequency kinetic energy sources. The power management system (PMS) aims to enhance the output characteristics of a TENG to be able to stabilise output voltage, increase current and actuate small electronic devices.

The literature review focused on recent advancements in sustainable and self-sufficient nano-energy power sources, particularly the TENG. Previous research aimed to optimise the TENGs structure, materials, and output performance. Various design adaptations and modifications were proposed including multilayered stack designs and use of artificial intelligence techniques for parameter optimisation. Incorporating a PMS plays a crucial role in optimising TENGs output performance. Strategies such as charge boosting, AC to DC conversions, impedance matching, and voltage regulation were identified. These methods aim to maximise energy output, convert AC to DC, match electrical energy with a load, and stabilise the TENGs output voltage.

This study uses a Voltage Multiplier Circuit (VMC) connected to capacitor, and an LTC3588 energy harvester chip. Evaluation occurred at four different stages: TENG device, VMC, LTC3588 energy harvester chip, and the PMS. Each stage was evaluated independently and as an entire system. Performance was tested under ideal and real-world conditions. Acquired data was validated through statistical analysis, including the 95th percentile assessment and standard deviation over a sample size. These were performed to highlight variability and dispersion across datasets.

Results of the evaluation process demonstrate that the voltage was stabilised, current increased to milliamps, and the PMS successfully powered small electronic devices. Objectives of the study research were met, demonstrating the effectiveness of the designed PMS. This research contributes to the development of sustainable power sources for various applications. Further research can focus on implementing the PMS on a larger scale.

## DECLARATION

I certify that this thesis:

1. does not incorporate without acknowledgment any material previously submitted for a degree or diploma in any university.
2. and the research within will not be submitted for any other future degree or diploma without the permission of Flinders University; and
3. to the best of my knowledge and belief, does not contain any material previously published or written by another person except where due reference is made in the text.

Signature of student.....*tanisha soldini*.....

Print name of student: Tanisha Rose Soldini

Date: 16/10/2023

I certify that I have read this thesis. In my opinion  it is/is not (please circle) fully adequate, in scope and in quality, as a thesis for the degree of Bachelor of Engineering (Robotics) (Honours) / Master of Engineering (Electronics). Furthermore, I confirm that I have provided feedback on this thesis and the student has implemented it minimally/partially  fully (please circle).

Signature of Principal Supervisor.....*Youhong Tang*.....

Print name of Principal Supervisor: Prof. Youhong Tang

Date: 16/10/2023

## **ACKNOWLEDGEMENTS**

Acknowledgements are made to academic supervisor Professor Youhong Tang and PhD student Yunzhong Wang for their unwavering support and invaluable guidance throughout the project. Successful completion of project will be made possible by the valuable contribution of the engineering service team, who provide the necessary components and equipment.

## LIST OF FIGURES

Figure 1: Structure and working principle of triboelectric nanogenerator. Structure of an integrated generator in the bending and releasing process [3].....	14
Figure 2: (a) Output voltages and (b) output currents of a two-layer structured TENG with gap sizes of 0.5 and 1.5 cm, and a three-layer structured TENG with and without a ground connection. Two-layer TENG is comprised of two aluminium outer electrodes (grey layers) with a mesoporous polymer film (green layer) attached to the top electrode. Gold nanoparticles, represented by the red particles are embedded on the bottom electrode. Three-layer TENG is comprised of two aluminium outer electrodes (grey layers) with a mesoporous polymer film (green layer) attached to the top electrode. The middle layer is made of an aluminium film coated by gold nanoparticles [19]. .....	16
Figure 3: Voltage and charge readings of TENG with alternating thickness and frequency (a) Output voltage waveforms of the TENG, (b) transferred charges in the TENG, (c) open-circuit output voltages, and (d) the short-circuit currents of TENG with PI interlayers [20]. .....	17
Figure 4: Comparison of the simulation and experimental results (a) temporal response of current for $R = 8$ Megaohms, (b) temporal response of the voltage for $R = 8$ Megaohms, (c) maximum current, and (d) maximum voltage [21]. .....	18
Figure 5: PMS with excitation TENG, bridge rectifier and switching system [25]. .....	19
Figure 6: PMS - charge pumping method (a) structural illustration of external charge excitation (ECE)-TENG, (b) electric circuit of ECE-TENG and (c) simplified working components of ECE-TENG [26]. .....	20
Figure 7: Rectification PMS, (a) rectification process, (b) bridge rectifier circuit diagram and (c) self-doubled rectification circuit diagram [33]. .....	22
Figure 8: Inductive-capacitive oscillating circuit PMS (a) inductive-capacitive switching circuit design and (b) stored energy in the external capacitor [40]. .....	24



Figure 9: General Process of Power Management System using Charge Pumping Method...	27
Figure 10: Single-Electrode TENG Device .....	28
Figure 11: Voltage Multiplier Circuit Diagram. Cascading form of voltage doublers of the cross-coupled switched capacitors. Current direction is dependent on the AC input signal. ..	29
Figure 12: Circuit Configuration of LTC3588 Energy Harvester Chip. Input Capacitor connected to $V_{in}$ . Output Capacitor connected to $V_{cc}$ . .....	31
Figure 13: Circuit Diagram of Power Management System. Voltage Multiplier Circuit connected in Series with LTC3588 Energy Harvester Chip. ....	32
Figure 14: Voltage Data for Voltage Multiplier Circuit. Output Voltage of TENG is represented in blue. Output Voltage of Voltage Multiplier Circuit with TENG input is represented in red. Output Voltage of Voltage Multiplier Circuit with Ideal input is represented in green. ....	37
Figure 15: Voltage Data of Power Management System. Y axes is measured in voltage [V]. X axes is measured in time [s]......	37
Figure 16: Current Data of Power Management System. Y axis is measured in amperes [A]. X axis is measured in time [s]......	38
Figure 17: Output Power of Power Management System. Y axis is measured in Watts [W]. X axis is measured in time [s]......	39
Figure 18: Power Management System with LED Output. ....	40
Figure 19: Statistical Analysis of Voltage Data from Power Management System. (a) 95th Percentile Calculation of 10 datasets. (b) Standard Deviation of 10 datasets. ....	40
Figure 20: Statistical Analysis of Current Data of Power Management System. (a) 95th Percentile Calculation of 10 datasets. (b) Standard Deviation of 10 datasets. ....	41

## **LIST OF TABLES**

Table 1: Comparison of various Power Management Systems .....	25
Table 2: Numerical Comparison of Data .....	41

# INTRODUCTION

## Background

Electricity usage has increased rapidly with the rising demand for electrification of transportation and devices. Environmental protection regulations, such as carbon neutrality, is driving society to harvest electrical energy from renewable energy sources. Contributing to alleviating carbon emissions associated with fossil fuel generators has sparked significant interest in the field of energy harvesting technologies, particularly triboelectric nanogenerator (TENGs). The TENG is an energy converter that operates at low-frequencies and harnesses electrical energy from natural sources of kinetic energy. TENG effectively mitigates carbon emissions from daily energy needs, complying with environmental regulations while maintaining cost-effectiveness. The most serious bottleneck affecting TENG's widespread application is the unstable output voltage and low output current. These output characteristics are influenced by unstable input kinetic energy and the inherent characteristics of the TENG, respectively. This study details the research and advancements in integrating power management systems (PMSs) for optimising TENGs output performance. Analysing the various techniques and methods proposed to optimise output current, minimise the effect of unstable input kinetic energy, and improve output voltage stability. This research evaluates a range of existing and publicised PMSs involving charge boosting, alternating current (AC) to direct current (DC) rectifications, impedance matching and voltage regulations. By identifying the merits and demerits of these strategies, this discussion provides an understanding of the PMS designed for TENGs.

## Current Solutions

Current deployments of renewable energy sources such as wind turbines and solar PV are on the rise. Wind turbines generates electrical energy by using the aerodynamic force from the rotor. The fundamental principle of wind turbines involves designing the blades to optimise energy capture. The system comprises of rotor blades, hub, nacelle, and tower. As wind flows across the blade, lift, and drag forces are created from the air pressure across the two sides of the blades. Lift is stronger than drag and causes the rotor to spin. The kinetic energy in moving air is converted to mechanical energy. The rotor is connected to the generator, converting mechanical energy to electrical power.

Solar PV systems generate electricity by converting sunlight into electrical energy. The system consists of photovoltaic cells, made up of semiconductive materials that absorb energy from sunlight. When sunlight hits the PV cell, energy is absorbed and excites the electrons in the semi-conductive materials, resulting electricity generation.

## **Triboelectric Nanogenerator (TENG)**

A triboelectric nanogenerator, also known as a TENG, is a renewable energy device. The name is derived from the triboelectric effect that uses two materials of different electron affinities undergoing a contact and separation motion. This motion causes the charges on the materials surface to be exchanged creating an electrical potential difference, generating electricity. The device is designed to harvest electrical energy from low-frequency range of kinetic energy found in the natural environment. Despite being a viable source of renewable energy, its mass production and application have been hindered by its low output performance. Characterised by low output current and unstable output voltage.

## **Objectives**

The overarching goal of this study is to develop a PMS for a TENG. This objective can be broken down into specific needs, each with their own set of requirements:

1. Stabilise Output Voltage
  - a. System must stabilise output between 5V – 12V.
2. Enhance Output Current
  - a. System must increase the output current from microampere level to usable range.
3. Power Electronic Devices
  - a. System must actuate commercial devices.

By meeting these specific needs and requirements, the PMS will be able to effectively utilise the output of the TENG for various applications.

## **Project Scope**

The proposed project aims to design, optimise, and evaluate a PMS for harvesting nano-energy. Primary objective is to investigate the effectiveness of a PMS with a TENG by enhancing

output voltage stability and increasing output current. Enabling the system to power electronic devices. The project scope involves researching and experimenting with a PMS connected to TENG technology to assess efficiency and design optimisation. The project aims to provide insight to potential applications and scalability of nano-energy harvesting technology for use in powering electronic devices. Evaluation methods commenced with connecting the PMS to a single-electrode TENG, two TENGs, and in an ideal environment. Employing charge pumping methods and commercial chips, a PMS through unique circuit connections is designed.

## **Outline**

The report is structured as follows: Introduction, Literature Review, Methodology, Results, Discussion and Conclusion. In the opening section, the significance, and objectives of the research problem are highlighted. The literature review offers a comprehensive analysis of existing knowledge on PMS for harvesting nano-energy and identifies the limitations of the research. Methodology proposes the research design, evaluation procedures, data collection and analysis methods required to achieve the objectives. Results graphically and numerically show the findings outlined in the research. Discussion section compares results to the objectives and literature. Limitations of the study are considered providing different avenues for future research. The final chapter summarises key findings, reiterating the importance of PMSs for harvesting nano-energy and the solutions they provide.

# LITERATURE REVIEW

## 1. Triboelectric Nanogenerator (TENG) Mechanism

Recent technological advancements have produced sustainable and self-sufficient nano-energy power sources for harvesting energy from the environment. Among these developments is a Triboelectric Nanogenerator (TENG), a system that harvests electrical energy from low-frequency range of kinetic energy from natural sources [1, 2]. The key feature of TENG technology is no carbon emissions during electricity generation. Promoting a more environmentally sustainable approach in comparison to conventional energy sources.

The concept of TENG is first proposed by Wang's group in 2012 [3]. The mechanism of TENG is the coupling of triboelectrification and electrostatic induction on two different electron affinity materials. The electron transfer between two material surfaces induced the triboelectrification and electrostatic symptoms to generate an electrical difference [4]. The prototype of this TENG consists of two aluminium (Al) alloy films which serve as electrodes surrounding polyethylene terephthalate (PET) and Kapton layers. Material choice is critical to the TENG operation, as they pose inherent elasticity characteristics that enable conversion of kinetic energy to electrical energy. Due to an external force, the triboelectric charge is induced on the surface of the material. The triboelectric effect facilitates charge transfer between the PET and Kapton layers. An opposite-direction waveform is generated once the TENG is released from the external force, forming a complete AC waveform.




Figure 1 has been removed due to Copyright Restrictions.

## **2. Current solutions through optimisation of TENG materials and structures**

While the TENG device can be a viable source of renewable energy, its production and application have been hindered by its limited output characteristics which are identified by unstable output voltage and low output current [5]. Previous research has predominantly focused on optimising the device's structure to collect more kinetic energy from the environment or improving the responsibility rate. For instance, creating multilayered stack TENG to increase the electrical output [6]. The layered design enhances energy conversion efficiency of the TENG as each layer contributes to the charge generation and transfer process, leading to a higher power output [7]. In addition, the selection and optimisation of materials contributes to enhancing electrical output. Several design adaptations and modifications of physical properties, such as increasing contact area and artificial fabricated material to supply ordinary surface charge density were researched [8-14]. For example, artificially injecting ions such as corona discharge to maximise the charge density of the material in a short period [15-18].

Improving output performance through device structure was another way to enhance the TENG output performance. In 2016, Chun *et al.* investigated boosting the output performance of a TENG through the electric double-layer effect [19]. In addition to the two triboelectric layers, a middle layer with an Al film coated by gold nanoparticles was inserted into the TENG device. Testing the three-layer TENG with a load resistance of 10 Mohm and an external force from 10 N to 90 N. As displayed in Fig. 1, the output voltages increase from 150 V to 355 V, and the current is enhanced from 0.095 mA to 1.5 mA, respectively. This is due to an increase in the surface contact area, resulting in a larger surface charge density, as shown in Fig. 2.

Figure 2 has been removed due to Copyright Restrictions.

An adaptation of Chun's group work was conducted in 2022 by Xin *et al.* Instead of adding a separate layer, Xin *et al.* adapted the current TENG design and inserted an interlayer into the triboelectric material. Polyamide (PI) was added to the triboelectric material altering the thickness to observe its effects on output performance. The TENG was subjected to frequencies of 4, 6, and 8 Hz with a separation distance of 2 mm. Results indicated that TENG performance exhibited an increase in output performance as the thickness of the PI layer decreased, as shown in Fig. 3(c) and 3(d). At an excitation frequency of 4 Hz, the PI interlayer thickness of 0.05 mm showed an output voltage five times larger than the TENG without PI interlayers as depicted in Fig. 3(c) [20].



Figure 3 has been removed due to Copyright Restrictions.

In more recent developments, researchers have increasingly turned to using artificial intelligence (AI) techniques in combination with TENG devices. Khorasand *et al.* utilised AI to find the optimal output performance for TENG parameters [21]. Specifically investigating load resistance, contact area, and thickness of triboelectric films to improve output energy and average power distribution. The AI system is a simulated program which updates the parameters by means of a population-based stochastic optimisation technique – co-evolutionary two-particle swarm optimisation method in parallel. Programmed through MATLAB, this method functions by two coded loops: (1) the internal loop which seeks to optimise variables in a predefined search space, (2) the external loop which accounts for penalty limitations. Comparisons between experimental results and simulations, presented in Fig. 4, has demonstrated the effectiveness of AI in optimising TENG parameters. Numerical investigation revealed that the selection of a proper value for the external resistor could increase the average power output to 18.21 mW at each cycle. The results reveal that the output energy of TENGs is dependent on load resistance, contact area, and dielectric film thickness. Notably, the maximum voltage is found to be independent of the contact area under open-circuit conditions. The current exhibits a linear relationship with the contact area during short-circuit

conditions. Furthermore, the resistor is identified as the dominant factor influencing the behaviour of sliding-mode TENG.

Figure 4 has been removed due to Copyright Restrictions.

### **3. Recent progress of power management system adopted in TENG.**

Recent methods involve the development of a PMS to enhance the output performance of a TENG. A PMS is integrated into a TENG to optimise, stabilise, and regulate the electrical energy harvested. The PMS can enhance the output current and stabilise the output voltage to provide DC output to power electronic devices. Furthermore, the PMS will filter any output which does not satisfy the output required to improve reliability and robustness.

#### **3.1.TENG Charge Boosting**

The most common PMS for optimising TENG output is charge boosting. Two main methods of charge boosting exist: maximising the energy output of TENG per cycle, and charge pumping. The maximised energy in a single working cycle can be determined by the cycles for maximised energy output (CMEO) of TENG. In 2013, Cheng *et al.* proposed the use of a pulsed TENG with a serial mechanism switch to realise the CMEO. Connection to the switch caused the energy stored in the TENGs intrinsic capacitor to discharge with the output current

following a similar discharge curve [22]. In comparison to TENG devices without a PMS, the output power provides a stable output voltage. Under experimental conditions, the TENG with a load resistance of 500 Ohms enhance the output current to 0.53 A and increases the power to 142 W in comparison to a standard TENG. However, the extra mechanical switch increases default risk and fabrication costs. A possible solution to improve the current design is a self-powered switch triggered by TENG's voltage, for example, an electrostatic vibrator switch and an air-discharge switch have been implemented in previous designs [23, 24].

In 2021, Yang *et al.* proposed a PMS based on charge pumping and CMEO TENG. The design used the TENGs' intrinsic capacitor as a variable component that is dependent on the overlapped area of its electrodes. The PMS of an excitation TENG, full bridge rectifier, booster circuit and stabilizer, and a main TENG is illustrated in Fig. 5. The charges are transferred between the main TENG and buffer capacitor, where the excitation TENG provides charges to the main TENG to increase charge density. Output current is rectified by either the full bridge rectifier or booster circuit, resulting in separated charges of opposite magnitude on the main TENG electrodes. Variability of capacitance in the main TENG in contrast to the constant capacitance of the buffer capacitor results in a voltage differential. This voltage difference facilitates the transfer of positive and negative charges between the main TENG and buffer TENG, generating electrical energy at both loads. Once more, a Zener diode is to prevent current flow back to the main TENG and conducts only when the output voltage of the main TENG reaches the breakdown voltage in the diode. Numerical results indicate that the proposed design reduces the output voltage of the system by 63.9% and increases the output current by 43.3% [25]. The voltage booster circuit with a switch circuit elevates charge density but reduces the peak output.




Figure 5 has been removed due to Copyright Restrictions.

Lui *et al.* employed a charge pumping strategy using a self-charging excitation nanogenerator and a voltage multiplier circuit. The proposed concept utilised an integrated charge excitation, where directly excited charges on the electrodes are transferred between the TENG intrinsic capacitor and external capacitors in the PMS. This system consists of a booster circuit, external charge excitation (ECE) TENG and main TENG. The booster circuit utilises a voltage-multiplier circuit consisting of diodes and capacitors to boost output, depicted in Fig. 6(b). A Zener diode is connected to prevent current flow back and conducts only when the output voltage of the main TENG reaches the breakdown voltage in the diode. The booster circuit is connected to excite TENG to induce a ‘self’ excitation TENG [26]. Further adaptations of the charge-boosting approach involve self-charge excitation nanogenerators. This structural enhancement eliminates the need for an excitation TENG by attaching a self-voltage multiplying circuit to a single electrode TENG, simplifying the PMS.

Figure 6 has been removed due to Copyright Restrictions.

The diode conducts when the TENG reaches its breakdown voltage. This is due to the diode’s voltage-dependent behaviour. As the voltage across the diode continues to increase and exceeds the breakdown voltage, the diode enters a state of reverse breakdown. During this state, the diode conducts in reverse bias causing the current to flow in the opposite direction (cathode to anode) [27]. Once the diode enters the breakdown state, it continues to conduct if the voltage across it remains above the breakdown voltage. However, if the diode operates in the breakdown condition for extended periods, or there are no limiting currents, it can result in excessive power dissipation and an increase in heat generation causing potential damage to the diode [27].

### 3.2. AC to DC Conversions

AC to DC conversions utilise full-wave and half-wave rectification circuits. It is a low efficient method for energy transfer due to the voltage drop across the diode and rectifier used for TENG output conversion. The PMS is divided into three sections: (1) the alternating current to alternating current (AC/AC) conversion; (2) the alternating current to direct current (AC/DC) conversion; and (3) the direct current to direct current (DC/DC) conversion. For instance, Cheng's group and Xi's group separately proposed synchronous switching mechanisms for AC/AC conversions of TENG [28, 29]. While Ghaffarinejad's group exponentially enhanced the energy conversion during AC/AC conversion using a Bennet's doubler circuit [30]. Furthermore, a charge supplemental channel was designed by Xu's group which the zero-checked TENG with a parallel diode in each cycle to prevents overloading and enhances the output performance [31].

An analysis by Niu *et al.* showed that the TENG device can be modelled as a series connection between a voltage source and a capacitor [32]. Once the AC output of TENG passes through the full-wave rectifier, the negative phase waveform will change to the positive phase resulting in a waveform of doubled frequency. Apart from it, the full-wave rectifier will have an increase in voltage loss due to the extra diodes required. In comparison to a half-wave rectifier, the circuit suffers fewer voltage losses due to the fewer diodes. While the conversion efficiency is half of the full-wave rectifier as the negative phase signal is ignored. Conversely, Xu *et al.* proposed an AC-to-DC conversion system to optimise the output performance of TENG. Using a self-doubled rectification TENG (SDR-TENG) device, the operation is separated into two periods. During the first period, charges are accumulated in the TENG's intrinsic capacitor. In the second period, these charges are released to the load, detailed in Fig. 7. This operation doubles the equivalent voltage of the total transferred charges, resulting in a two-times increase in output energy and a two-times increase in output power. During this operation, the energy loss caused by the asymmetric output is solved by combining the positive and negative output from the rectifier. Optimising the rectification method allows the PMS to be compatible with other designs of AC/AC and DC/DC conversions of TENG [33]. Based on superposition, the output voltage is doubled in comparison to the input. As output power is proportional to the square of voltage, it can be increased by a maximum of four times.

Figure 7 has been removed due to Copyright Restrictions.

Notably, SDR-TENG is implemented using two diodes and is compatible with other power management strategies. Through simulation and experimentation of SDR-TENG, significant improvement of energy output was observed for large resistive loads and small capacitive loads. In comparison to charge pumping, the above three strategies require an extra regulator. Accurate calculations are needed for choosing a suitable regulator to satisfy the output requirements. Depending on TENG output characteristics, variable input of the power management will increase the risk of default due to the feasibility of the input voltage being less than the regulator's trigger voltage.

### **3.3. Impedance Matching**

Zhu *et al.* proposed a power management circuit using inductive and capacitive transformers for impedance matching [34]. The circuit design consists of a rectifier, capacitors, a regulator, and an electromagnetic transformer. This circuit reduces the TENGs high voltage providing a 5 V constant voltage and DC output. Notably the coil turn ratio of the transformer is a critical factor in determining the induction transformer. Pu *et al.* investigated the number of turns in a coil to achieve an impedance match between electrical energy and the battery. Through the design of an inductor transformer, Pu *et al.* discovered that a coil ratio of 24.4 and 36.7 can reduce charging time to 23 minutes and 10 minutes respectively [35]. Maintaining a discharge capacity of 10.7 mAh and 0.4 mAh which is equivalent to 81.1% and 70.5% of the complete charge. Impedance matching between the electrical energy and battery is reduced to

approximately 110 Ohms. Current output increases from 2 mA to 73.5 mA and voltage decreases from 391.4 V to 9.2 V.

Similarly, in 2014, Han *et al.* designed an induction transformer to enhance output current and improve the stability of output voltage [36]. Output current increases to 45 mA which is a 15% rise from the original current output, and matching impedance reduces the magnitude by three ratings in comparison to the TENGs direct output. Park's group buck converter included a shared inductor to alter the DC voltage to 70 V from TENG [37]. Power conversion efficiency improved to 70.7% with a reduction in capacitance at the switching node, which is 21.15% higher than previous investigations. The induction transformer, functioning as a TENG's permanent magnet synchronous motor, offers several benefits such as improved voltage conservation efficiency, matching impedance reductions, and increased current. As the transformer ratio is fixed, the proposed design cannot suit a range of different TENGs due to its variable output. Transformers utilised for buck conversion show a reduction in matching impedance and facilitate the conversion of high voltage and low current to low voltage and high current. Induction transformers are ideal for high-frequency TENG, while PMSs based on capacitive transformers have no requirements on working frequency for TENGs. In 2014, Tang *et al.* proposed a new TENG design utilising a power-transformed-and-managed TENG (PM-TENG). The design operates with a mechanical switch that causes a set of capacitors to change their connection between series and parallel, charging and discharging, respectively. For TENGs, when operating with a capacitor transformer, the voltage can be decreased while the current and charges are increased. Under experimental conditions, the results demonstrate that the number of capacitors placed in the circuit reduces output voltage and increases output charges. The power supply also shows a significant increase when charging a 10-microfarad capacitor [38].

### **3.4. Voltage Regulation**

Energy loss during the conservation stage is a serious bottleneck that needs to be addressed by the development of PMSs. Particularly, limiting is the energy storage efficiency that occurs due to losses experienced on the energy transfer between the TENGs intrinsic capacitor and an external capacitor. To reduce these losses and manage the high-voltage output of a TENG, Zhang *et al.* proposed a two-stage conditioning system without requiring an external control system. The first stage utilises a Bennet doubler for signal rectification. The second stage

consists of a self-actuated electrostatic switch and a DC/DC buck converter [39]. The use of a Bennet doubler is implemented to overcome the saturated voltage experienced in a half-wave rectification. As a result, the maximum energy harvested per cycle is limited. Bennet doubler increases the voltage across the capacitor and transducer, leading to a higher TENG output. In comparison to a traditional full-wave bridge rectifier, the proposed TENG shows an improvement of converted energy by 24 times. The output voltage maintains a threshold of 20V and is compatible with commercial regulators.

In 2017, Cheng *et al.* proposed an inductance-capacitance (LC) oscillating circuit design to transfer energy between the TENG and external capacitor. The design minimises energy loss during transfer owing to the energy stored in the main capacitor. Once the voltage stored in the capacitor reaches the switch's trigger voltage, the stored energy will transfer to the load. A bridge rectifier is implemented into the PMS to convert TENGs AC output to DC. The circuit adopts a serial-switch design based on a voltage-charge plot to lower resistance for maximised energy outputs per cycle. The switch is triggered by the TENG's peak voltage, and energy is transferred to the primary inductor when the switch is on. Conversely, when the switch is off, energy is transferred from the inductor and stored in the external capacitor. More than 72% AC to DC power conversion efficiency was obtained. Experiment results reveal an LC oscillating circuit's ability to enhance TENG output performance. Lu *et al.* conducted experiments with different capacitive values ranging from  $1 \mu F$  –  $1000 \mu F$  and observed a 2640 times improvement in stored energy using an LC oscillating circuit with a  $1000 \mu F$  load capacitor, as shown in Fig. 8. Furthermore, the LC oscillating circuit improved overall stability [40].

Figure 8 has been removed due to Copyright Restrictions.



## 4. Comparison

Charge boosting offers a high adaptability strategy through charge accumulation. However, the strategy can require an additional TENG as an input source leading to a complex structure and increase risk of default. Based on bridge rectifiers, the AC to DC rectifiers require a high input from the TENG as large amounts of power are lost from the voltage drop across the diode and leakage current. However, the combination of the half-wave rectifier and Bennet doubler allows fewer losses during the conversion stage. This can alleviate some issues of TENGs charging efficiency. Voltage regulation requires the use of a trigger voltage in a switching mechanism. The regulator will only operate once the input voltage is higher than the switch's trigger voltage. Additionally, most regulators require pre-stored power. This is not suitable for long standby modes due to leakage current in the entire system and accumulation of heat on the regulator. Once the pre-stored power no longer exists, the PMS does not function. Finally, using transformers for impedance matching is an effective method for improving energy supply efficiency. However, due to the variability in working ranges, i.e., impedance matching operating at high frequencies and TENG functions at low-frequency wave conditions, impedance matching is not an ideal solution. Table 1 compared the merits and demerits of various PMSs.

*Table 1: Comparison of various Power Management Systems*

Power management strategy	MERIT	DEMERIT
Charge boosting	<ul style="list-style-type: none"> <li>▪ High adaptability</li> </ul>	<ul style="list-style-type: none"> <li>▪ Requires an extra self-excitation TENG.</li> <li>▪ Relative complex structure</li> </ul>
AC to DC rectification	<ul style="list-style-type: none"> <li>▪ Produces high energy efficiency.</li> </ul>	<ul style="list-style-type: none"> <li>▪ High output requirement of TENG</li> </ul>
Voltage regulation	<ul style="list-style-type: none"> <li>▪ Less voltage losses</li> </ul>	<ul style="list-style-type: none"> <li>▪ Unstable output voltage</li> </ul>
Impedance matching	<ul style="list-style-type: none"> <li>▪ Efficient energy transfer.</li> <li>▪ Maximum amount of power can be delivered.</li> </ul>	<ul style="list-style-type: none"> <li>▪ Generates a distorted output.</li> <li>▪ Accurate calculation required to choose correct regulator</li> </ul>

## 5. Conclusion

This literature review aims to improve understandings of the PMSs implemented to improve the output performance of a TENG. Findings demonstrate the significant impact effective

PMSs have on maximising energy transfer, minimising energy loss and improving stability. Through evaluation and analysis of previous research, this review has publicised a range of methodologies for the challenges of TENGs output performance. Each approach has merit and demerits with the choice of PMS on chosen parameters and requirements of the application. The review discussed the effectiveness of the PMS in optimising output efficiency. Voltage regulator circuits have shown improvements in energy transfer, while notable enhancements in AC to DC power conversion efficiency. Impedence matching has proven worthy in optimising system energy transfer efficiency, maximising power transfer and minimising energy loss. Additionally, energy storage units are crucial to assist in the stabilisation of the system output when the input is unstable. Based on the comparison of four different PMSs, charge boosting is the most suitable choice for harvesting electrical energy from low-frequency range kinetic energy. The wide operation range and simple circuit provide robustness after the operation period. Furthermore, charge boosting's simple circuit will reduce fabrication, maintenance, and repair costs. Substantial contributions in TENG energy harvesting systems research exist, but there are still several avenues for future research and development. Research must focus on real-world applications, optimising the long-term performance of TENG, ensuring compatibility and scalability with various TENG configurations, and identifying the necessary materials for practical use. Continued progress in this field shows promise in satisfying the demand for electrical energy and presents new possibilities for energy harvesting technologies.

# METHODOLOGY

## General Process

TENG technologies can harvest natural kinetic energy, converting it into electrical energy. The output signal from TENG, being in the form of an alternating signal (AC), requires rectification to direct current (DC) prior to being boosted by the Voltage Multiplier Circuit (VMC). The DC outputs from the VMC are integrated into the LTC3588 energy harvester chip, which utilises the resulting output to power various electronic devices. The general process used is outlined in Fig. 9.

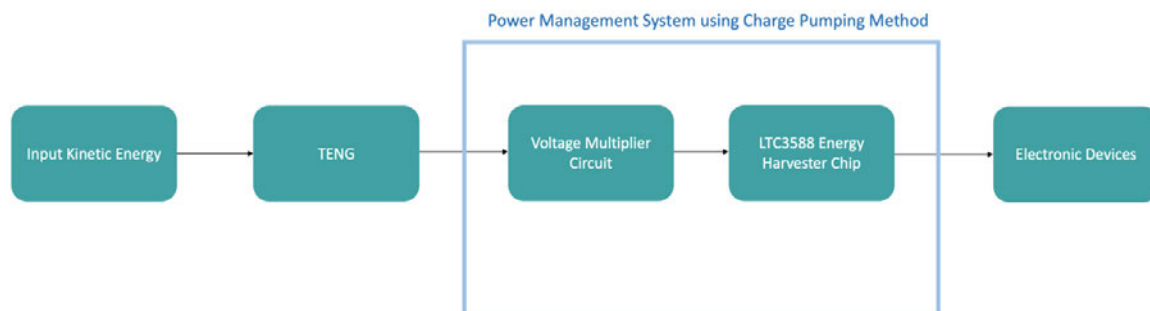


Figure 9: General Process of Power Management System using Charge Pumping Method

## Assumptions and Constraints

The PMS intends to rectify AC signal to DC signal through diodes. This rectification process assumes input is a sinusoidal waveform with a fixed frequency. Limited to the positive half-cycle of the AC voltage, resulting in a DC output that is lower than the input – due to the voltage drop across resistor diodes. Failure in rectification may result from overheating or overvoltage of diodes and capacitors. Regular maintenance and proper cooling of components is necessary to prevent such failures.

The integrated electronic circuit will be used to manage the electrical energy from TENG stabilising output voltage waveform, enhancing output current to a useable range with increased efficiency. The unstable input voltage from TENG may burn the electronic components due to exceeding the maximum constraints. Serial connected capacitors and diodes are required for a voltage multiplier to prevent failure from unstable high voltage in the TENG. Voltage multiplier smooths the voltage waveform, avoiding short circuit, and fix current direction preventing triboelectric material failure due to dielectric breakdown.

Increasing output current to a usable range is vital to power electronic devices. Current is boosted through a commercial chip (LTC3588), and nonrated inputs will be unable to activate electronic device and sensors.

The PMS may generate voltage and current fluctuations, which can affect electronic device performance. There is an assumption that the PMS can deliver power without overloading or overheating. Compatibility with electronic devices and adherence to manufacturer's specifications are recommended to prevent damage or malfunction. In conjunction with regular maintenances and testing to help identify and prevent potential failures.

### **Triboelectric Nanogenerator (TENG) Device**

Fabricated through 3D printing, the TENG device illustrated in Fig. 10 features a circular structure with a diameter of 60mm. The device's surface is designed with stratified composition with a layer of copper (Cu) and polytetrafluoroethylene (PTFE). Small half-circle of Cu is implemented as the second electrode. It is vital that the Cu does not remain in continuous contact with the PTFE layer, as it impedes the effective transfer of charges during the contact and separation motion. The specific design of this TENG device was developed by PhD Student Yunzhong Wang [41].

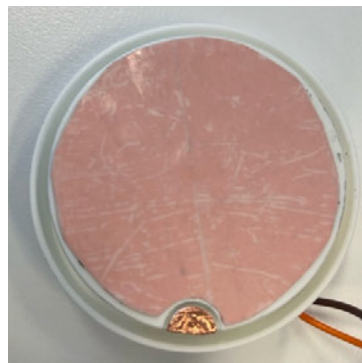


*Figure 10: Single-Electrode TENG Device*

Nitrile rubber was chosen as one of the triboelectric materials for its opposing position in the triboelectric material series [42]. This optimises the devices performance in generating electrical charges.

### **Charge Pumping Method**

Charge pumping is a concept of switched capacitor circuits – comprised of capacitor and switches such as clock-controlled field-effects transistors (FETS) [43]. These circuits function

by timing and controlling these switches to manage the input voltage polarity determined under the capacitors transfer characteristics.

The charge pumping method was selected to enhance TENG output performance due to its ability to operate with low current levels generated from the device and avoidance of excitation TENG or switches. Rendering it the most viable and efficient solution for single-electrode TENGs. The charge pumping method has potential to result in a high peak-to-peak open circuit voltage, which ensures that the TENG output can be increased to an adequate voltage for operation [44].

### Voltage Multiplier Circuit

Based on the charge pumping technique, a Voltage Multiplier Circuit (VMC) was created. Diodes are used to control current flow instead of a manual switch. A VMC is an electronic circuit used to multiply the voltage of an AC input signal. Fig. 11 displays the general form consisting of a series of diodes and capacitors connected in a series of parallel configuration.

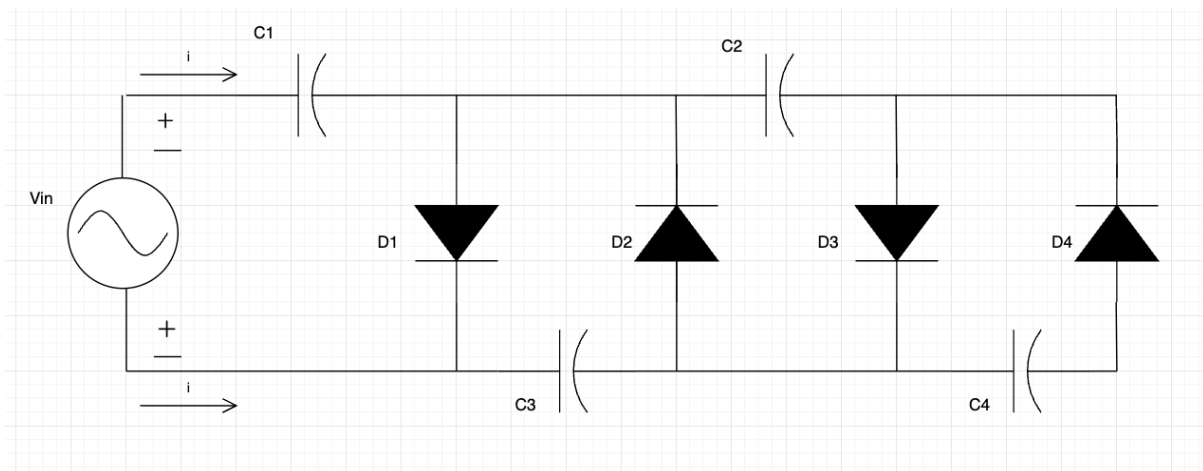


Figure 11: Voltage Multiplier Circuit Diagram. Cascading form of voltage doublers of the cross-coupled switched capacitors. Current direction is dependent on the AC input signal.

An AC input is applied to the first stage (classified as one diode and one capacitor) of the circuit. Current direction is dependent on polarity of input voltage. During the positive half-cycle of the input voltage, diodes allow current flow and signal rectification producing a half-wave waveform. The rectified signal is filtered by the capacitors which charges to the peak voltage of said signal. During the negative half-cycle of the input voltage, the diodes block current flow and capacitors discharge to provide a smoothed DC output [44].

Subsequent stages consist of additional diodes and capacitors connected in parallel to the first stage. The voltage across this capacitor is added to the previous stage doubling the output voltage each time. DC output is the sum of voltage stored in each capacitor in the circuit. Number of stages increase; output voltage multiplies accordingly [45, 46].

## **LTC3588 Energy Harvester Chip**

To aid in voltage regulation and increase current, the LTC3588 energy harvester chip, designed by Linear Technology, efficiently converts, and manages energy from various ambient sources has been used in this study [47].

Key features of LTC3588 are detailed:

1. Energy Harvesting Capabilities.

Component is specifically designed to harvest energy from low-power sources, making it suitable for the TENG device where energy availability is limited.

2. Wide Input Voltage Range.

Component can accept input voltages from 2.7 V to 20 V, accommodating to the varying outputs of TENG (depending on TENG size, frequency, material, and output from voltage multiplier circuit) [48].

3. Energy Storage.

Integrates an energy storage element for continuous power supply. Contains a supercapacitor to store backup energy and small capacitors to eliminate ripple noise.

4. Low Quiescent Current

Designed to consume minimal power when idle, helping to maximise energy utilisation and extend operability of stored energy.

5. Compact Form Factor.

Small and compact device makes it suitable for integration into various portable products.

6. Customisation Options.

External resistors or pins allows adaption of chips behaviour for specific application needs.

The energy harvester chip integrates a low-loss full-wave bridge rectifier with a high efficiency buck converter to form a complete energy harvesting solution optimised for high output impedance energy sources. The phenomenon wherein energy transfer between two capacitors

incurs energy loss is referred to as the two-capacitor paradox [47]. Presence of internal capacitors can result in energy consumption when two capacitors are connected – LTC3588 energy harvester chip does not suffer from this issue [49].

This chip was chosen for its ability to input a 950nA current which complements the VMC and TENG outputs. Fig. 12 details circuit configuration of LTC3588. An input and output capacitor of  $1\mu F$ . These capacitors are placed for voltage regulation and energy storage [46].

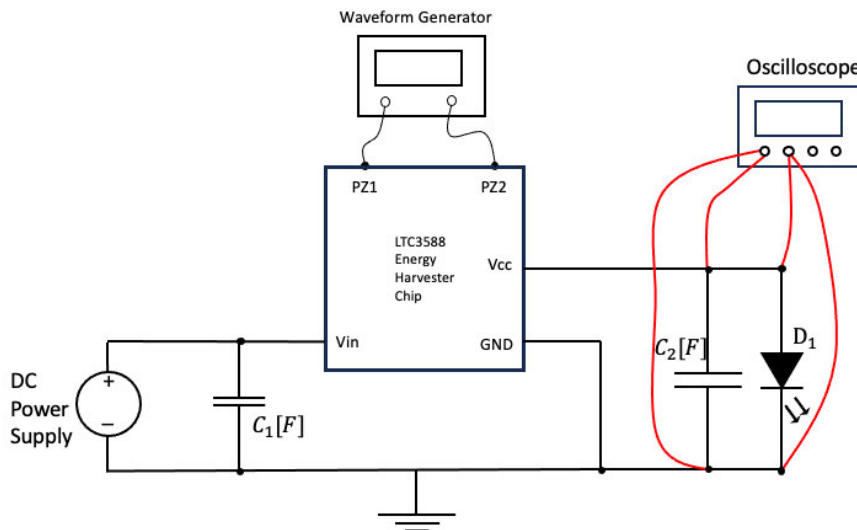


Figure 12: Circuit Configuration of LTC3588 Energy Harvester Chip. Input Capacitor connected to  $V_{in}$ . Output Capacitor connected to  $V_{cc}$ .

## Power Management System

The VMC was attached in series to the DC input of the energy harvester chip to form the PMS, illustrated in Fig. 13. VMC is connected in series to capacitor and LTC3588 energy harvester chip for voltage sharing abilities. Output capacitor is placed at  $V_{cc}$  to store and regulate voltage.

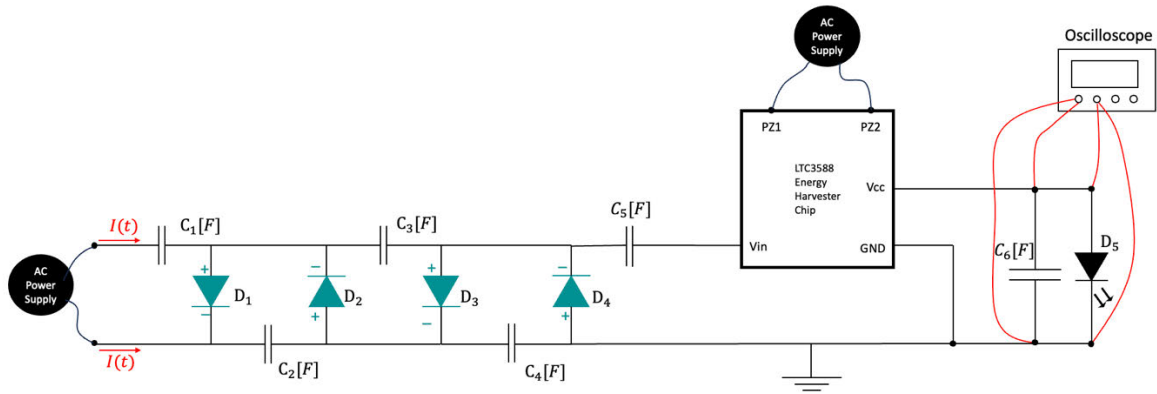


Figure 13: Circuit Diagram of Power Management System. Voltage Multiplier Circuit connected in Series with LTC3588 Energy Harvester Chip.

## Equipment and Setup

Experiment was conducted at Tonsley in Laboratory 1.13 from June to September. Testing was conducted at a standard temperature range of 20° to 25°.

Provided in the laboratory, the Keysight InfiniiVision MSO-X 2004A oscilloscope used to measure and analyse analogue and digital signals from the PMS. Using standard 10:1 passive voltage probe for signal measurements the oscilloscope presented these signals on an 8.5inch colour TFT LCD display. Equipped with multiple functions, the ‘save/recall’ button on the oscilloscope was used to store data via USB connectivity. Each waveform was recorded with a time frame of 10 seconds [50].

For producing controlled waveforms, the Keysight Technologies 33500B Series Waveform Generator was used. This waveform generator was used simulate ‘ideal’ testing, creating a baseline for data comparison. It was configured to generate a sinusoidal waveform with a frequency of 2.5Hz with an amplitude of 4Vpp and output impedance set to high. These values were determined based on the TENG testing. Waveform configuration was facilitated through the front panel controls [51].

To deliver precise and regulated power to the LTC3588 energy harvester chip, the Keysight Technologies U8031, a triple output DC power supply was used. This power supply-controlled input voltage levels. Featuring 3 channels and a 4-digit LED display for voltage and current readings. Front-knobs and a digital interface were used to adjust and monitor the digital inputs



to the energy harvester chip to simulate an ‘ideal’ environment. Banana jacks are used to connect the digital power supply to the circuit [52].

The Keysight Technologies U3401A, a dual display multi-meter, was used for measuring resistor resistance. Featuring a dual display with 4 ½ digits allows for accurate and clear readings. Equipped with standard banana jacks to ensure secure and reliable connections, the resistance values were determined for implementation into the circuit. For observing the resistance values, the ‘ohm’ button was used [53]. Specifications of each equipment is detailed in Appendix A.

## **Evaluation Procedure**

Evaluating the PMS occurred in four stages.

1. E1: TENG device.
2. E2: Voltage Multiplier Circuit
3. E3: LTC3588 Energy Harvester Chip
4. E4: PMS

Evaluation of TENG was conducted independently to establish a benchmark comparison. VMC and LTC3588 energy harvester chip were subjected to individual assessments to confirm functionality. Complete evaluation of the PMS is the combination of the energy harvester chip and VMC.

Evaluation methods, E2, E3 and E4 were applied to TENG and ideal inputs. A waveform generator was used for ideal testing, design, and theoretical analysis. It assisted in establishing a baseline understanding of the circuit’s behaviour and performance under ideal conditions. The experimental input (TENG) was used to simulate real-world scenarios and influencing factors such as noise, interference, and fluctuations. The TENG validates the PMSs ability to function under operational conditions, assess robustness, reliability, and conformity to specified standards. Ensuring that the PMS meets intended objectives and functions optimally. Evaluation procedures were repeated ten times for statistical analysis. Utilising Nitrile rubber as a triboelectric material, through contact and separation with the TENG device, data was recorded for 10 seconds interval. An oscilloscope was used to measure the output voltage across the output capacitor.

A shunt resistor was placed to measure electric current, by measuring the voltage drop across the resistor. The current value is derived from Ohm's law (1) by using the shunt resistor's known resistance [54].

$$V = I \cdot R \quad (1)$$

Shunt resistor of 1 kilohm was chosen for its high precision and accuracy in current measurement applications [54]. This ensures that the measured current is reliable and consistent. The resistor value strikes a balance between precision and voltage impact.

### **E1. TENG**

Appendix B. details the TENG device circuit diagram. Output of TENG is connected to a 680pF capacitor. Voltage across the capacitor is read by the oscilloscope.

### **E2. Voltage Multiplier Circuit**

Appendix C. details the connection of the VMC and its power source, either the TENG or an ideal source. To match the TENG device's output characteristics, the circuit was designed with four stages and an output capacitor. First two capacitors have a capacitance of 330pF each, while the subsequent three capacitors have a 680pF capacitance. These values were determined based on the TENGs output to attain the requisite voltage threshold for optimal performance. Circuit was tested with the TENG device where it produced an output through contact and separation motion. Voltage was read from the output capacitor. Data was recorded for ten second intervals at a low frequency.

### **E3. LTC3588 Energy Harvester Chip**

Appendix D. details the energy harvester chip and its power source, either TENG device or ideal source. Like Fig. 12 capacitors are placed for voltage regulation and energy storage. Voltage was read from the output capacitor. Data was recorded for ten second intervals at a low frequency.

### **E4. Power Management System**

Appendix E. details the PMS and its power source, either ideal source or TENG device. Similar to Fig. 13 the VMC was attached in series to the DC input of the energy harvester chip. Voltage was read from the output capacitor. Data was recorded for ten second intervals at a low frequency. Appendix F. shows the PMS circuit.

## Processing Data

USB connectivity, supported by the Oscilloscope, allowed for data collection and storage as excel spreadsheets. Voltage values were obtained through output capacitors and current values through resistors. Power (2) was determined using the root mean square (RMS) voltage and current values. Following formula was applied:

$$P = I \cdot V \quad (2)$$

Each excel spreadsheet was imported into a Python script – attached in Appendix G. Python version 3.8 was used to import voltage and current data. Due to noise interference, the data was filtered by a low pass Butterworth filter. This filter was used for its ability to pass low-frequency signals and attenuates high-frequency signals. Butterworth filter was configured with following parameters:

- |                             |                           |                     |
|-----------------------------|---------------------------|---------------------|
| ▪ Sampling frequency: 30 Hz | ▪ Cut off frequency: 2 Hz | ▪ Filter order of 2 |
|-----------------------------|---------------------------|---------------------|

After filter, the data is plotted along axis of time and amplitude. Following packages were used for data manipulation:

- |              |          |
|--------------|----------|
| ▪ NumPy      | ▪ Pandas |
| ▪ Matplotlib | ▪ SciPy  |

To ensure validity of results, statistical analysis occurred over a repeated data set of sample size ten. Data was subjected to standard deviation and 95<sup>th</sup> percentile calculations presented as bar graphs – attached in Appendix H. Numerical values are presented in a Table for comparison.

## Experimental Errors

When conducting experiments with circuitry and electrical instruments, several potential sources of experimental errors can emerge. Temperature fluctuations can affect the characteristics of electronic components such as resistors and capacitors. To ensure minimal effect, the circuit remained in the same environment, maintaining a stable temperature during testing. Improper grounding can introduce unwanted noise and interference to the measurements. Proper grounding and use of differential measurements were used to minimise this error. This limits the electromagnetic interference and noise reduction of nearby sources. Instruments used were monitored and calibrated periodically to ensure accuracy of results.

# RESULTS

## Results

Results chapter is divided four sections: (1) Voltage Recordings, (2) Current Recordings, (3) Power Data, and (4) Validation of Results. Methods of validation include calculating the 95<sup>th</sup> percentile and statistical analysis. Digital Oscilloscope was used to obtain data and is stored onto a USB as an excel spreadsheet. Voltage recordings are obtained from the output capacitor. Current recordings are obtained through a shunt resistor. Power is calculated from experimental data. All graphs include TENG and ideal inputs.

## Voltage Recordings

Voltage data was obtained from the voltage multiplier circuit and PMS. The VMC focused on stabilising the voltage.

### *Voltage Multiplier Circuit*

Fig. 14 show voltage data for the VMC. Output voltage of TENG is represented in blue. Output voltage of VMC with TENG input is represented in red. Output voltage of VMC with ideal input is represented in green. TENG voltage output oscillates around the zero-point, with few peaks approaching 1V. Output voltage of the VMC demonstrates an increase in voltage reaching maximum voltage of 6V. Repetition of peak voltage values indicates the waveform's stability, as it does not exceed a 0.5V fluctuation between peaks.

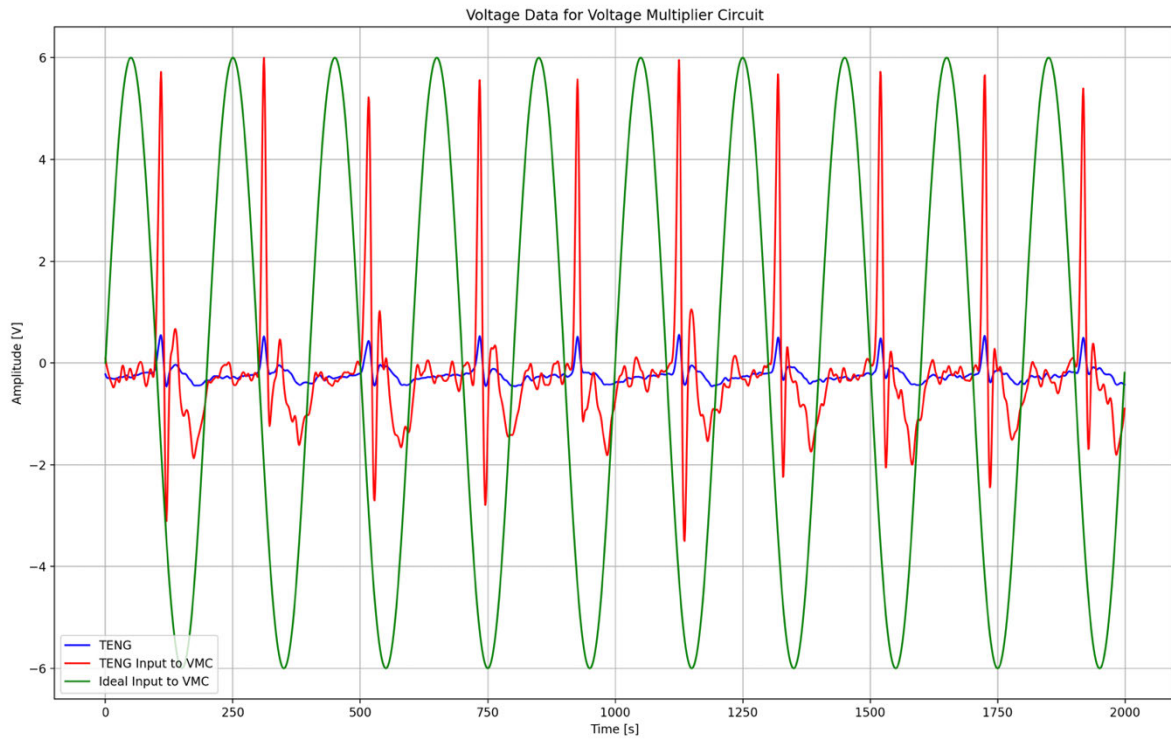


Figure 14: Voltage Data for Voltage Multiplier Circuit. Output Voltage of TENG is represented in blue. Output Voltage of Voltage Multiplier Circuit with TENG input is represented in red. Output Voltage of Voltage Multiplier Circuit with Ideal input is represented in green.

## Power Management System

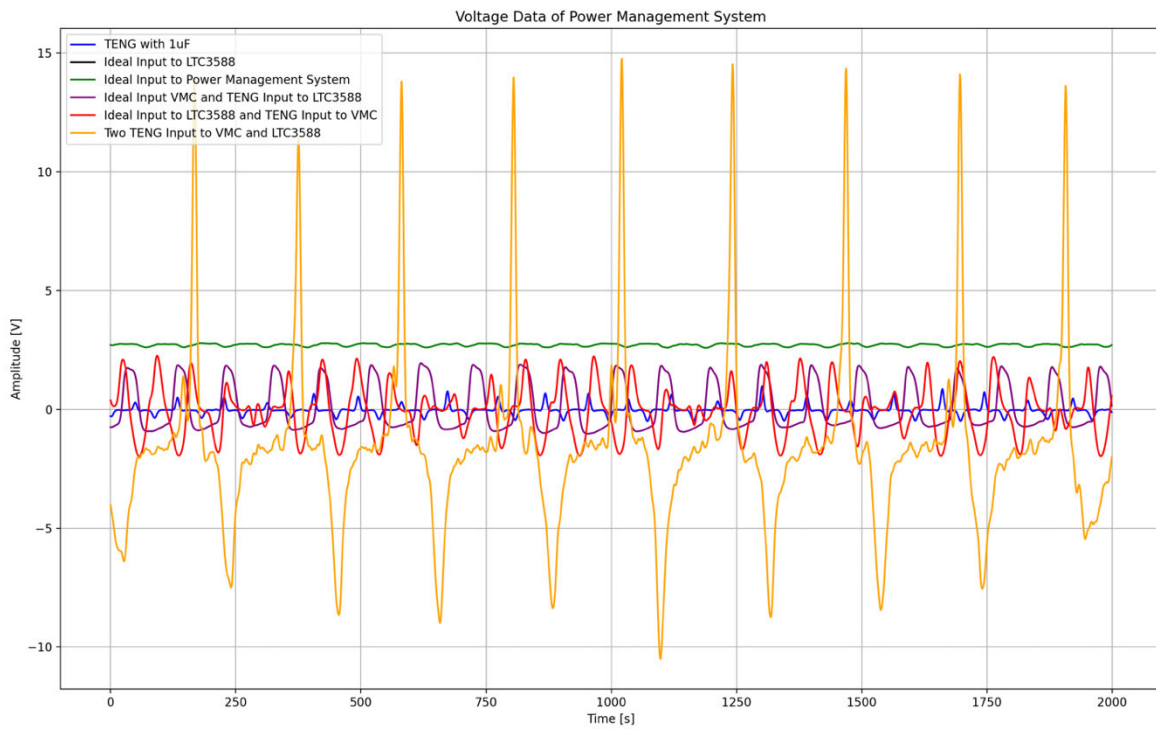


Figure 15: Voltage Data of Power Management System. Y axes is measured in voltage [V]. X axes is measured in time [s].

Fig. 15 displays voltage data of PMS. The most prominent observation is the output voltage of PMS with two TENG inputs – represented in orange. Comparing to TENG voltage – outlined in blue – the PMS output voltage has significantly increased to a peak of 16.2V. Similar to Fig. 14 the voltage has increase and stabilised.

### Current Recordings

Current data was collected from the PMS. The LTC3588 energy harvester is responsible for affecting current. As VMC has no impact on current values it is excluded from recordings. Assessment of current data is focused on the PMS.

### Power Management System

Fig. 16 shows current data of the PMS. Most current waveforms oscillate near the origin. Among them, the red waveform represents an ideal input to the LTC chip and TENG input to the VMC, deviating from origin into milliampere (mA) range. Detailed in orange, two TENG input to the PMS produces peak current values of 23.5 mA.

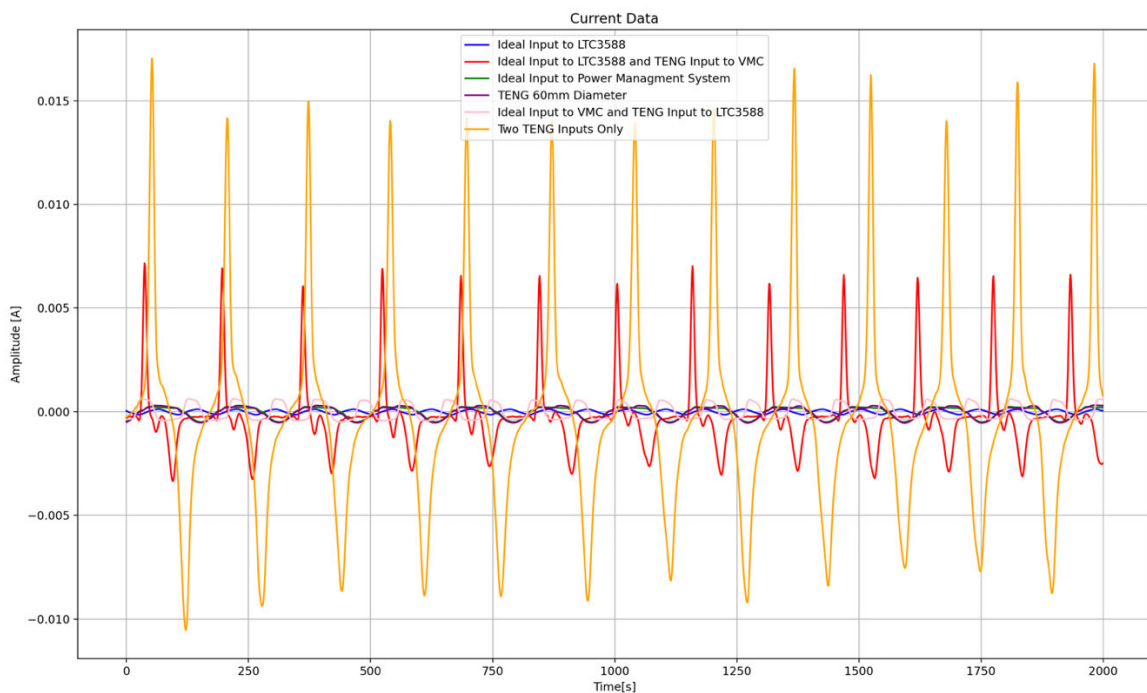


Figure 16: Current Data of Power Management System. Y axis is measured in amperes [A]. X axis is measured in time [s].

### Power Recordings

Power recordings were obtained using the power equation (2). RMS current and voltage values obtained through the shunt resistor were used for power calculations.

## Power Management System

Fig. 17 displays power data of the PMS. Detailed in orange, two TENG input to the PMS produces power values up to 0.38W. Fluctuations of 0.1W in the data. These fluctuations are influenced by the irregular current waveform.

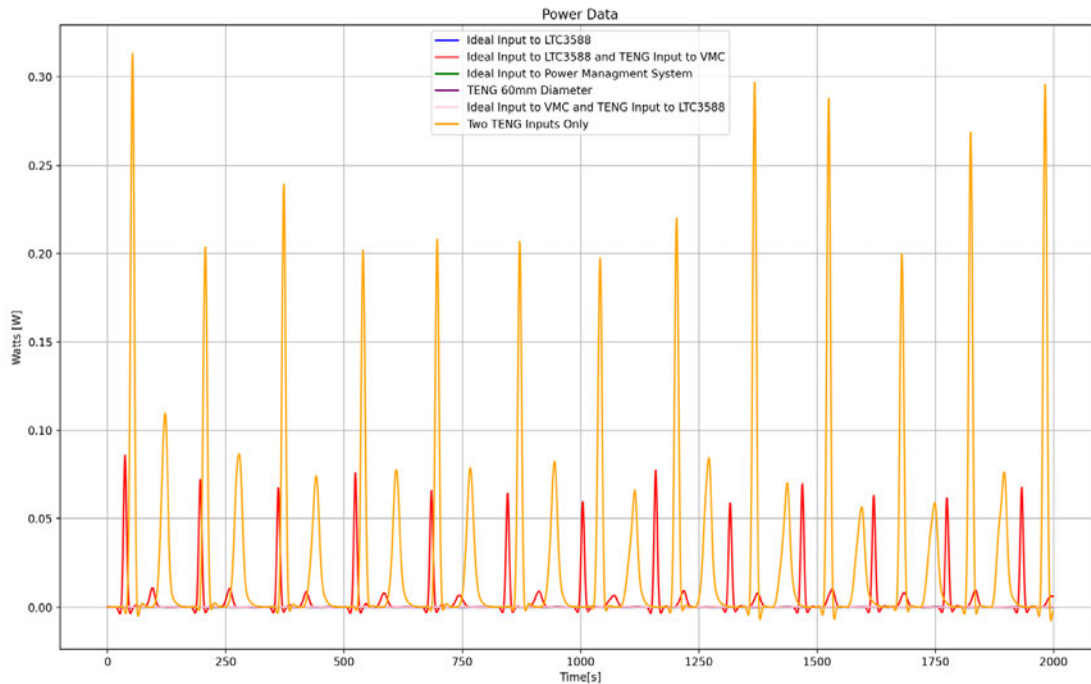


Figure 17: Output Power of Power Management System. Y axis is measured in Watts [W]. X axis is measured in time [s].

## Visual Representation

Fig. 18 illustrates the PMS with an illuminated LED, comprising an ideal input and TENG input. The TENG input is directed to the VMC, and the ideal input is connected to the LTC3588 energy harvester chip. Observing Fig. 18 it is evident that the research's objective to power small electronic devices has been achieved.

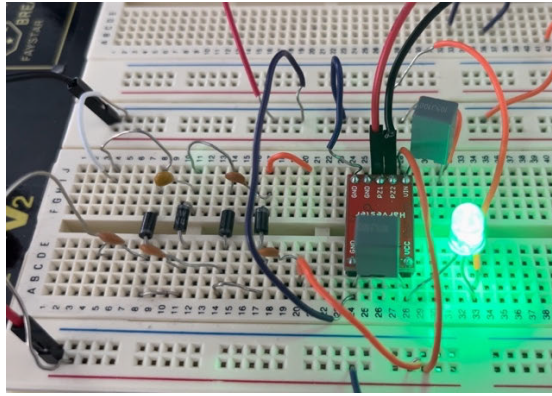


Figure 18: Power Management System with LED Output.

## Statistical Analysis

Statistical analysis was conducted on voltage and current data. Standard deviation and 95<sup>th</sup> percentile were used to provide insight into the distribution and variability in the data recorded.

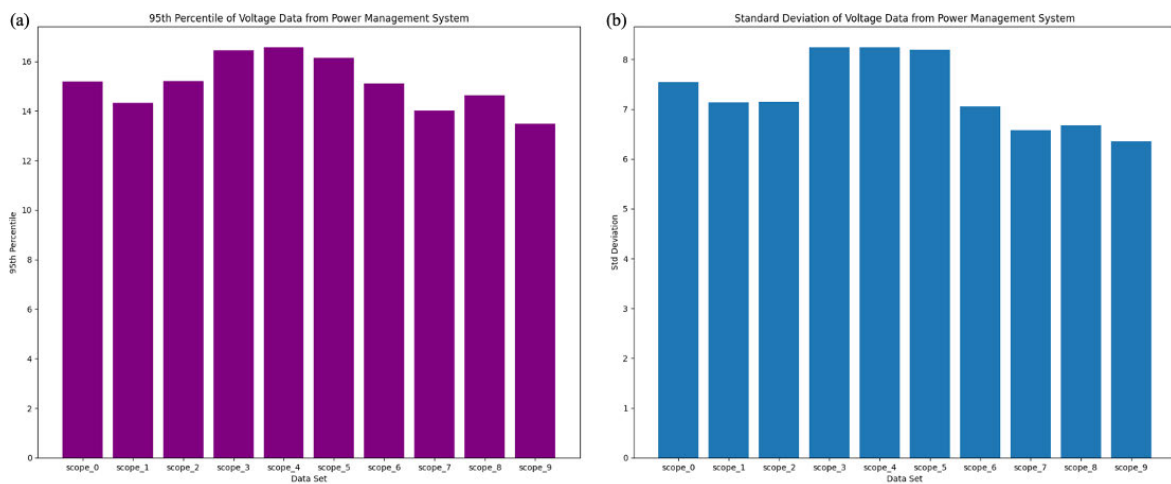


Figure 19: Statistical Analysis of Voltage Data from Power Management System. (a) 95<sup>th</sup> Percentile Calculation of 10 datasets. (b) Standard Deviation of 10 datasets.

Fig. 19 presents the 95<sup>th</sup> percentile (a) and standard deviation (b) of voltage data from the power management system. All datasets have similar standard deviations and 95<sup>th</sup> percentile values, highlighting the uniformity in variability and dispersion across the dataset. The uniformity suggests a comparable distribution shape for the data.



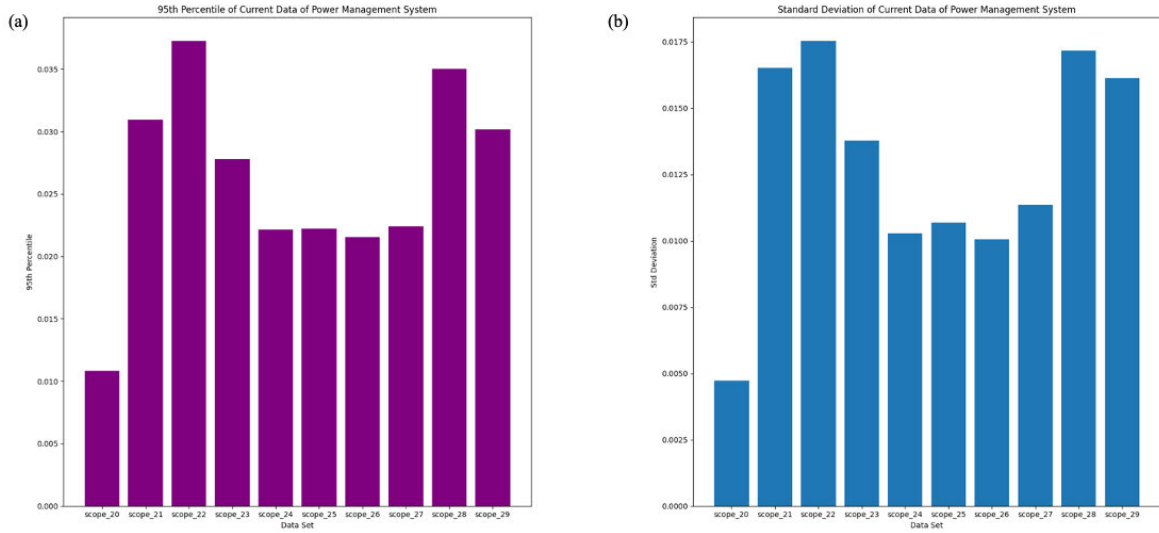


Figure 20: Statistical Analysis of Current Data of Power Management System. (a) 95th Percentile Calculation of 10 datasets. (b) Standard Deviation of 10 datasets.

Fig. 20 shows the 95<sup>th</sup> percentile (a) and standard deviation (b) of voltage data from the power management system. In certain datasets, comparable levels of variability and dispersion are observed, with greater fluctuations in remaining datasets. These fluctuations can be attributed to variations in input voltage, resulting from testing two TENG devices in a non-controlled environment. These external factors can influence results.

Table 2: Numerical Comparison of Data

Evaluation Method	Voltage [V]	Current [mA]	Power [W]
TENG	▪ 0.579	▪ 0.0625	▪ 3.61e-5
Voltage Multiplier Circuit (TENG Input)	▪ 6.2	▪ 0.045	▪ 2.79e-4
PMS (TENG Inputs)	▪ 16.2	▪ 23.5	▪ 0.38

Table 2 provides a comparison of maximum voltage, current and power values obtained through different evaluation methods. The LTC3588 energy harvester chip was excluded from comparison as it is a commercial design intended for integration into the PMS. Results solely obtained from the chip were used to confirm functionality.

PMS presented the largest increase in voltage, current and power with values reaching 16.2V, 23.5 mA and 0.38 W, respectively. VMC displayed an increase in voltage compared to the TENG device but did not exhibit an increase in current. As power is a factor of current and voltage, it did not significantly increase.

## Discussion

This study aimed to design, optimise, and evaluate a PMS for harvesting nano-energy. The system incorporates a VMC and LTC3588 energy harvester chip. Four methods of evaluation were used. Each stage contributed to understanding the system's performance, from individual components to final integrated system.

The most significant findings are the system's ability to stabilise voltage, increase output current and power small electronic devices. These outcomes meet the research objectives. Fig. 14 details the voltage data from the VMC and TENG. Each peak correlates to the moment at which both triboelectric materials come into contact and charges are transferred. The frequency of peaks correlate to the rate at which contact-separation of TENG occurs. As the TENG is to be employed in low-frequency ranges the TENG maintained a 2-3Hz frequency. Voltage output from VMC resembles the waveform of the TENG output but with a larger amplitude. The similarity in waveforms indicates that the VMC performs as its intended function. The VMC is employed to enhance the TENGs output voltage to ensure compatibility with the LTC3588 energy harvester chip, which requires a minimum input voltage of 2.7V. Fig. 15 details the output voltage of the PMS, demonstrating its stabilisation and increase to a peak of 16.2V.

The LTC3588 energy harvester chip is a popular tool for piezoelectric renewable devices, but its usage in TENG applications is limited. Ma *et al.* conducted a study that used the energy harvester chip to power wireless sensors, producing a current consumption of 4 mA and output voltage of 20V [55]. Comparatively, the PMS results in Table 2 achieved a maximum output voltage of 16.2V. Noted that the current produced by the PMS was significantly higher at 23.5mA. This difference in current values could be qualified to variations in the input to LTC3588 energy harvester chip.

Fig. 17 displays power data of the PMS Detailed in orange, two TENG input to the PMS produces power values up to 0.38W. Fluctuations of 0.1W in the data. These fluctuations are influenced by the irregular current waveform. Statistical analysis confirmed the variability and dispersion of data. Wang *et al.* performed a study incorporating the LTC3588 energy harvester chip to a hybridised TENG and Piezoelectric-Electromagnetic (PEG) vibration mechanism. The system demonstrated an output power of 6.5mW when excited at low frequencies [56].

Voltage stabilisation is crucial for converting nano-energy into a useable form. The TENG device is not suitable for direct use as the output voltage is unstable. Integration of VMC helps address this challenge and stabilises the output voltage. Capacitors are used to maintain a medium voltage across the output. At higher voltages, the capacitor charges causing the output voltage to decrease. At lower voltages, the capacitor discharges causing an increase in output voltage. This approach offers a practical solution for converting unpredictable and low-voltage nano-energy into a consistent and usable power source.

Ideal input was attached to VMC with the at TENG input the LTC chip. This ensured that the LED could be turned on within a time frame. Based on de Fazio *et al.* findings, the capacitor took 1600 minutes to charge completely and power the LED attached [57]. Due to limited accessibility to laboratory, it was necessary to have a continuous supply to the VMC. Ma *et al.* utilised the energy harvester chip to power wireless sensors using a piezoceramic patch bonded to a low-frequency vibration beam. The LTC3588 energy harvester chip was used to transfer and collect energy. Use of switching mechanisms between energy harvester chip and sensor, a 0.33F supercapacitor was charged for 12hr by the harvested vibrational energy [55].

Limited literature investigates the output current from an LTC3588 energy harvester chip powered by TENG devices. Investigations have been conducted using the LTC3588 energy harvester chip with piezoelectric devices, but the output current is not mentioned [58, 59]. Based on the datasheet, the LTC3588 energy harvester chip, when used with a TENG device can provide up to 100 mA of continuous current. Specific output is dependent on the TENG device.

The PMS was able to increase current to a usable level as shown in Fig. 16. Multiple nano-energy sources generate microampere currents that are insufficient for practical applications. The PMS's ability to amplify current provides possibilities for powering electronic devices that were previously difficult to operate with nano-energy sources.

Noted that the LTC3588 cannot have fast activation because the supercapacitor is directly connected to the storage capacitor. Since there is not enough voltage to turn on the buck converter, in the beginning, this chip takes a long time to charge the supercapacitor and storage capacitor for activation voltage (5V). The research methodology including use of TENG input and ideal testing with a waveform generator, enabled a comprehensive evaluation of the PMS.

Providing insights to a controlled and uncontrolled environment, considering factors such as noise and interference.

The methodology applied has several strengths and weaknesses. The VMC can boost the voltage generated from the TENG device. It is advantageous as the TENG voltage output is too low to operate with the required input voltage of the LTC3588 energy harvester chip. It ensures a consistent and usable voltage for charging. However, it can introduce efficiency trade-offs at high voltage conversions due to leakage current and component limitations. Balancing voltage increase with energy efficiency is crucial. To assist balancing, optimising the number of stages in the VMC was important. Efficiency can decrease with an increased number of stages [60]. Increasing frequency of contact-separation motion can increase the power loss due to parasitic capacitance and reactance [61].

Incorporation of energy harvester chip allows for efficient conversion of voltage to a usable energy output, ensuring minimal energy loss in the process. This integration between the VMC and LTC3588 energy harvester chip adds complexity to the system and increases cost.

Statistical analysis and filtering techniques enhances data validity, they do not reduce the impact of noise on results, remaining a potential limitation. Therefore, maintaining a balance between noise reduction and information preservation is crucial for determining accurate conclusions from data. As results demonstrate promise, certain uncertainties and questions remain. Long-term stability and reliability of system in diverse environmental conditions should be investigated. Additionally, scalability to meet higher energy demands and adaptivity to various triboelectric materials requires further investigation.

Combination of the VMC and LTC3588 energy harvester chip has demonstrated significant potential for optimising and harvesting nano-energy. Results of this study provides solutions for practical applications of harvesting nano-energy to power small electronic devices.

## CONCLUSION

This study has presented the design, optimisation, and evaluation of a PMS tailored for efficiently harvesting nano-energy. Evaluating several circuit designs with the TENG device and ideal inputs it was determined that the projects objectives were achieved. The VMC has stabilised the output voltage at 6V. Combination of LTC3588 energy harvester chip and VMC increased current to milliamps and actuated small electronic devices. Data was validated through statistical analysis of standard deviation and 95<sup>th</sup> percentile calculations, demonstrating the datasets variability and dispersion. Visual testing occurred through an LED at the output.

The PMS exhibited the largest increase in voltage, current and power with values reaching 16.2V, 23.5mA and 0.38W, respectively. The VMC demonstrated an increase in voltage compared to the TENG device reaching a maximum of 6.2V but did not exhibit an increase in current. As power is a factor of current and voltage, it did not significantly increase. Voltage values were stabilised within a 0.5V range of fluctuations. Visual testing of the PMS was successful, confirmed by illumination of LED at output. These results exhibit promise in the chosen field, yet certain uncertainties and refinement of irregular current waveforms remain.

The PMS effectively stabilised voltage levels, increase current to milliamperes and demonstrated the capability to power small electronic devices. These outcomes successfully met the study's objectives.

The research contributes valuable insights to the field of harvesting nano-energy, particularly in the development of PMSs for practical applications. It highlights the potential of nano-energy sources in powering low-energy electronic devices. Emphasising the importance in design and evaluation in optimising energy harvesting systems. The ongoing investigation into sustainable energy solutions through nano-energy demonstrates promise in reducing dependency on conventional power sources – promoting environmental sustainability. Ongoing research remains vital to address uncertainties, improve scalability and expand adaptability to various operating conditions. Overall, this study marks a significant step toward harnessing nano-energy as a sustainable power source for emerging technologies.

## **FUTURE WORK**

Further work may involve expanding real-world testing and validation of the PMS. This could include evaluating the system's performance under different environmental conditions, such as temperature variations, humidity, or mechanical vibrations. Real-world testing can provide insight into the system's robustness, reliability, and its ability to operate in practical scenarios.

Further investigations can be made into exploring advanced energy storage technologies, such as supercapacitors or batteries. This can contribute to storing harvested energy more effectively and efficiently.

Future work can focus on scaling up the PMS for larger-scale energy harvesting applications. Involving the system design and optimising for higher power outputs and integrating into practical devices or systems.

## REFERENCES

- [1] Niu, S., & Wang, Z. L. (2015). Theoretical systems of triboelectric nanogenerators. *Nano Energy*, *14*, 161–192. <https://doi.org/10.1016/j.nanoen.2014.11.034>
- [2] Zhu, G., Peng, B., Chen, J., Jing, Q., & Lin Wang, Z. (2015). Triboelectric nanogenerators as a new energy technology: From fundamentals, devices, to applications. *Nano Energy*, *14*, 126–138. <https://doi.org/10.1016/j.nanoen.2014.11.050>
- [3] Fan, F.-R., Tian, Z.-Q., & Lin Wang, Z. (2012). Flexible triboelectric generator. *Nano Energy*, *1*(2), 328–334. <https://doi.org/10.1016/j.nanoen.2012.01.004>
- [3] Fan FR, Tian ZQ, Wang ZL. Flexible triboelectric generator. *Nano Energy* 2012; 1: 328–334. <https://doi.org/https://doi.org/10.1016/j.nanoen.2012.01.004>.
- [4] Wang, J., Zhou, L., Zhang, C., & Wang, Z. L. (2019). *Small-Scale Energy Harvesting from Environment by Triboelectric Nanogenerators*. [www.intechopen.com](http://www.intechopen.com); IntechOpen. <https://www.intechopen.com/chapters/65412>
- [5] Xue J, Zheng N, Zhao W, Cao X, Wang Z. Rubik-cube-based self-powered sensors and system: An approach toward smart toys, *Adv Funct Mater* 2022; 32: 202107099. <https://doi.org/10.1002/adfm.202107099>.
- [6] Zheng Y, Liu T, Wu J, Xu T, Wang X, Han X, Cui H, Xu X, Pan C, Li X. Energy conversion analysis of multilayered triboelectric nanogenerators for synergistic rain and solar energy harvesting. *Adv Mater* 2022; 34: 2202238. <https://doi.org/https://doi.org/10.1002/adma.202202238>.
- [7] Zhou H, Wei X, Wang B, Zhang E, Wu Z, Wang ZL. A multi-layer stacked triboelectric nanogenerator based on a rotation-to-translation mechanism for fluid energy harvesting and environmental protection. *Adv Funct Mater* 2023; 33: 2210920. <https://doi.org/https://doi.org/10.1002/adfm.202210920>.
- [8] Chun J, Kim JW, Jung W, Kang C-Y, Kim S-W, Wang ZL, Baik JM. Mesoporous pores impregnated with Au nanoparticles as effective dielectrics for enhancing triboelectric nanogenerator performance in harsh environments. *Energy Environ Sci* 2015; 8: 3006–3012. <https://doi.org/10.1039/C5EE01705J>.
- [9] Zhang X-S, Han M-D, Wang R-X, Meng B, Zhu F-Y, Sun X-M, Hu W, Wang W, Li Z-H, Zhang H-X. High-performance triboelectric nanogenerator with enhanced energy density based on single-step fluorocarbon plasma treatment. *Nano Energy* 2014; 4: 123–131.

<https://doi.org/https://doi.org/10.1016/j.nanoen.2013.12.016>.

[10] Bai P, Zhu G, Zhou YS, Wang S, Ma J, Zhang G, Wang ZL. Dipole-moment-induced effect on contact electrification for triboelectric nanogenerators, *Nano Res* 2014; 7: 990–997.

<https://doi.org/10.1007/s12274-014-0461-8>.

[11] Song G, Kim Y, Yu S, Kim M-O, Park S-H, Cho SM, Velusamy DB, Cho SH, Kim KL, Kim J, Kim E, Park C. Molecularly engineered surface triboelectric nanogenerator by self-assembled monolayers (METS), *Chem Mater* 2015; 27: 4749–4755.

<https://doi.org/10.1021/acs.chemmater.5b01507>.

[12] Zhang J-H, Hao X. Enhancing output performances and output retention rates of triboelectric nanogenerators via a design of composite inner-layers with coupling effect and self-assembled outer-layers with superhydrophobicity. *Nano Energy* 2020; 76: 105074.

<https://doi.org/https://doi.org/10.1016/j.nanoen.2020.105074>.

[13] Zhang H, Quan L, Chen J, Xu C, Zhang C, Dong S, Lü C, Luo J. A general optimization approach for contact-separation triboelectric nanogenerator. *Nano Energy* 2019; 56: 700–707.

<https://doi.org/https://doi.org/10.1016/j.nanoen.2018.11.062>.

[14] Zhou L, Liu D, Zhao Z, Li S, Liu Y, Liu L, Gao Y, Wang ZL, Wang J. Simultaneously enhancing power density and durability of sliding-mode triboelectric nanogenerator via interface liquid lubrication. *Adv Energy Mater* 2020; 10: 2002920.

<https://doi.org/https://doi.org/10.1002/aenm.202002920>.

[15] Wang S, Xie Y, Niu S, Lin L, Liu C, Zhou YS, Wang ZL. Maximum surface charge Density for triboelectric nanogenerators achieved by ionized-air injection: Methodology and theoretical understanding. *Adv Mater* 2014; 26: 6720–6728.

<https://doi.org/https://doi.org/10.1002/adma.201402491>.

[16] Liu Y, Liu W, Wang Z, He W, Tang Q, Xi Y, Wang X, Guo H, Hu C. Quantifying contact status and the air-breakdown model of charge-excitation triboelectric nanogenerators to maximize charge density, *Nat Commun* 2020; 11: 1599. <https://doi.org/10.1038/s41467-020-15368-9>.

[17] Wang Y, Jin X, Wang W, Niu J, Zhu Z, Lin T. Efficient triboelectric nanogenerator (TENG) output management for improving charge density and reducing charge loss, *ACS Appl Electron Mater* 2021; 3: 532–549. <https://doi.org/10.1021/acsaelm.0c00890>.



[18] Wang J, Wu H, Fu S, Li G, Shan C, He W, Hu C. Enhancement of output charge density of TENG in high humidity by water molecules induced self-polarization effect on dielectric polymers. *Nano Energy* 2022; 104: 107916.

<https://doi.org/https://doi.org/10.1016/j.nanoen.2022.107916>.

[19] Chun J, Ye BU, Lee JW, Choi D, Kang C-Y, Kim S-W, Wang ZL, Baik JM. Boosted output performance of triboelectric nanogenerator via electric double layer effect, *Nat Commun* 2016; 7: 12985. <https://doi.org/10.1038/ncomms12985>.

[20] Xin C, Li Z, Zhang Q, Peng Y, Guo H, Xie S. Investigating the output performance of triboelectric nanogenerators with single/double-sided interlayer. *Nano Energy* 2022; 100: 107448.

<https://doi.org/https://doi.org/10.1016/j.nanoen.2022.107448>.

[21] Khorsand M, Tavakoli J, Kamanya K, Tang Y. Simulation of high-output and lightweight sliding-mode triboelectric nanogenerators, *Nano Energy* 2019; 66: 104115.

<https://doi.org/https://doi.org/10.1016/j.nanoen.2019.104115>.

[22] Cheng G, Lin Z-H, Lin L, Du Z, Wang Z.L. Pulsed nanogenerator with huge instantaneous output power density. *ACS Nano* 2013; 7: 7383–7391.

<https://doi.org/10.1021/nn403151t>.

[23] Cheng G, Zheng H, Yang F, Zhao L, Zheng M, Yang J, Qin H, Du Z, Wang ZL. Managing and maximizing the output power of a triboelectric nanogenerator by controlled tip-electrode air-discharging and application for UV sensing. *Nano Energy* 2018; 44: 208–216.

<https://doi.org/https://doi.org/10.1016/j.nanoen.2017.11.062>.

[24] Yang J, Yang F, Zhao L, Shang W, Qin H, Wang S, Jiang X, Cheng G, Du Z. Managing and optimizing the output performances of a triboelectric nanogenerator by a self-powered electrostatic vibrator switch. *Nano Energy* 2018; 46: 220–228.

<https://doi.org/https://doi.org/10.1016/j.nanoen.2018.02.013>

[25] Yang Z, Yang Y, Wang H, Liu F, Lu Y, Ji L, Wang ZL, Cheng J. Charge pumping for sliding-mode triboelectric nanogenerator with voltage stabilization and boosted current, *Adv Energy Mater* 2021; 11: 2101147.

<https://doi.org/https://doi.org/10.1002/aenm.202101147>.

[26] Liu W, Wang Z, Wang G, Liu G, Chen J, Pu X, Xi Y, Wang X, Guo H, Hu C, Wang ZL. Integrated charge excitation triboelectric nanogenerator. *Nat Commun* 2019; 10: 1426.

<https://doi.org/10.1038/s41467-019-09464-8>.

- [27] Evstigneev, M. (2022). Introduction to Semiconductor Physics and Devices (1st ed., Vol. 1, pp. 257–261) [Review of Introduction to Semiconductor Physics and Devices]. Springer. <https://doi.org/10.1007/978-3-031-08458-4>
- [28] Xi F, Pang Y, Li W, Jiang T, Zhang L, Guo T, Liu G, Zhang C, Wang ZL. Universal power management strategy for triboelectric nanogenerator. *Nano Energy* 2017; 37: 168–176. <https://doi.org/https://doi.org/10.1016/j.nanoen.2017.05.027>.
- [29] Cheng G, Zheng H, Yang F, Zhao L, Zheng M, Yang J, Qin H, Du Z, Wang ZL. Managing and maximizing the output power of a triboelectric nanogenerator by controlled tip–electrode air-discharging and application for UV sensing. *Nano Energy* 2018; 44: 208–216. <https://doi.org/https://doi.org/10.1016/j.nanoen.2017.11.062>.
- [30] Ghaffarinejad A, Hasani JY, Hinchet R, Lu Y, Zhang H, Karami A, Galayko D, Kim S-W, Basset P. A conditioning circuit with exponential enhancement of output energy for triboelectric nanogenerator. *Nano Energy* 2018; 51: 173–184. <https://doi.org/https://doi.org/10.1016/j.nanoen.2018.06.034>.
- [31] Xu L, Wu H, Yao G, Chen L, Yang X, Chen B, Huang X, Zhong W, Chen X, Yin Z, Wang ZL. Giant voltage enhancement via triboelectric charge supplement channel for self-powered electroadhesion. *ACS Nano* 2018; 12: 10262–10271. <https://doi.org/10.1021/acsnano.8b05359>.
- [32] Niu S, Zhou YS, Wang S, Liu Y, Lin L, Bando Y, Wang ZL. Simulation method for optimizing the performance of an integrated triboelectric nanogenerator energy harvesting system. *Nano Energy* 2014; 8: 150–156. <https://doi.org/https://doi.org/10.1016/j.nanoen.2014.05.018>.
- [33] Xu S, Zhang L, Ding W, Guo H, Wang X, Wang ZL. Self-doubled-rectification of triboelectric nanogenerator. *Nano Energy* 2019; 66: 104165. <https://doi.org/https://doi.org/10.1016/j.nanoen.2019.104165>.
- [34] Zhu G, Chen J, Zhang T, Jing Q, Wang ZL. Radial-arrayed rotary electrification for high performance triboelectric generator. *Nat Commun* 2014; 5: 3426. <https://doi.org/10.1038/ncomms4426>.
- [35] Pu X, Liu M, Li L, Zhang C, Pang Y, Jiang C, Shao L, Hu W, Wang ZL. Efficient charging of Li-ion batteries with pulsed output current of triboelectric nanogenerators. *Adv Sci* 2016; 3: 1500255. <https://doi.org/https://doi.org/10.1002/advs.201500255>.

- [36] Han C, Zhang C, Tang W, Li X, Wang ZL. High power triboelectric nanogenerator based on printed circuit board (PCB) technology. *Nano Res* 2015; 8: 722–730. <https://doi.org/10.1007/s12274-014-0555-3>.
- [37] Park I, Maeng J, Shim M, Jeong J, Kim C. A bidirectional high-voltage dual-input buck converter for triboelectric energy-harvesting interface achieving 70.72% end-to-end efficiency. in: 2019 Symposium on VLSI Circuits, 2019: pp. C326–C327. <https://doi.org/10.23919/VLSIC.2019.8778018>.
- [38] Tang W, Zhou T, Zhang C, Fan R, Han C, Wang ZL. A power-transformed-and-managed triboelectric nanogenerator and its applications in a self-powered wireless sensing node. *Nanotechnology* 2014; 25: 225402. <https://doi.org/10.1088/0957-4484/25/22/225402>.
- [39] Zhang H, Galayko D, Basset P. A conditioning system for high-voltage electrostatic/triboelectric energy harvesters using benet doubler and self-actuated hysteresis switch, In: 2019 20<sup>th</sup> International Conference on Solid-State Sensors, Actuators and Microsystems & Eurosensors XXXIII (TRANSDUCERS & EUROSENSORS XXXIII), 2019: pp. 346–349. <https://doi.org/10.1109/TRANSDUCERS.2019.8808359>.
- [40] Cheng X, Miao L, Song Y, Su Z, Chen H, Chen X, Zhang J, Zhang H. High efficiency power management and charge boosting strategy for a triboelectric nanogenerator. *Nano Energy* 2017; 38: 438–446. <https://doi.org/https://doi.org/10.1016/j.nanoen.2017.05.063>.
- [41] Wang, Y., Pham, A., Tohl, D., & Tang, Y. (2021). Simulation Guided Hand-Driven Portable Triboelectric Nanogenerator: Design, Optimisation, and Evaluation. *Micromachines*, 12(8), 955. <https://doi.org/10.3390/mi12080955>
- [42] Zhang, R., & Olin, H. (2020). Material choices for triboelectric nanogenerators: A critical review. *EcoMat*, 2(4). <https://doi.org/10.1002/eom2.12062>
- [43] *The Fundamentals of a Charge Pump Circuit - Technical Articles*. (n.d.). [Www.allaboutcircuits.com. https://www.allaboutcircuits.com/technical-articles/switched-capacitor-circuits-charge-pump-circuit-basics/](https://www.allaboutcircuits.com/technical-articles/switched-capacitor-circuits-charge-pump-circuit-basics/)
- [44] Jian, G., Meng, Q., Yang, N., Feng, L., Wang, F., Chen, Y., & Wong, C.-P. (2022). Superhigh charge density and direct-current output in triboelectric nanogenerators via peak shifting modified charge pumping. *Nano Energy*, 102, 107637. <https://doi.org/10.1016/j.nanoen.2022.107637>
- [45] *High boost converter using voltage multiplier*. (n.d.). [Ieeexplore.ieee.org](https://ieeexplore.ieee.org). Retrieved September 30, 2023, from <https://ieeexplore.ieee.org/abstract/document/1568967>

- [46] Brugler, J. S. (1971). Theoretical performance of voltage multiplier circuits. *IEEE Journal of Solid-State Circuits*, 6(3), 132–135. <https://doi.org/10.1109/JSSC.1971.1049670>
- [47] *LTC3588-1 Datasheet and Product Info* | Analog Devices. (2009). Analog.com. <https://www.analog.com/en/products/ltc3588-1.html>
- [48] Mixed-signal and digital signal processing ICs | Analog Devices. (2019). Analog.com. <https://www.analog.com/en/index.html>
- [49] Mita, K., & M. Boufaïda. (1999). Ideal capacitor circuits and energy conservation. *American Journal of Physics*, 67(8), 737–739. <https://doi.org/10.1119/1.19363>
- [50] Keysight. (n.d.). MSOX2004A Mixed Signal Oscilloscope: 70 MHz, 4 Analog Plus 8 Digital Channels. Keysight. Retrieved October 14, 2023, from <https://www.keysight.com/se/en/product/MSOX2004A/mixed-signal-oscilloscope-70-mhz-4-analog-8-digital-channels.html>
- [51] Keysight. (n.d.). *U8031A Triple-Output DC Power Supply, 30 V / 6 A (2x) and 5 V / 3 A; 375 W*. Keysight. Retrieved October 14, 2023, from <https://www.keysight.com/se/en/product/U8031A/triple-output-dc-power-supply-30v-6a-2x-5v-3a-375w.html#:~:text=U8031A%20Triple%20Output%20DC%20Power>
- [52] Keysight. (n.d.). *U3401A Digital Multimeter, 4½ Digit Dual Display [Obsolete]*. Keysight. Retrieved October 14, 2023, from <https://www.keysight.com/se/en/product/U3401A/digital-multimeter-4-digit-dual-display.html>
- [53] Keysight. (n.d.). 33500B and 33600A Series Trueform Waveform 20, 30, 80, 120 MHz PDF Asset Page | Keysight. [www.keysight.com](https://www.keysight.com). Retrieved October 14, 2023, from <https://www.keysight.com/se/en/assets/7018-05928/data-sheets/5992-2572.pdf>
- [54] *Measuring current with shunt resistors - Power Electronic Tips*. (n.d.). [www.powerelectronicstips.com](http://www.powerelectronicstips.com). Retrieved October 8, 2023, from <https://www.powerelectronicstips.com/measuring-current-shunt-resistors/>
- [55] Ma, Y., Ji, Q., Chen, S., & Song, G. (2017). An experimental study of ultra-low power wireless sensor-based autonomous energy harvesting system. *Journal of Renewable and Sustainable Energy*, 9(5), 054702. <https://doi.org/10.1063/1.4997274>. |
- [56] Wang, L., He, T., Zhang, Z., Zhao, L., Lee, C., Luo, G., Mao, Q., Yang, P., Lin, Q., Li, X., Maeda, R., & Jiang, Z. (2021). Self-sustained autonomous wireless sensing based on a hybridized TENG and PEG vibration mechanism. *Nano Energy*, 80, 105555. <https://doi.org/10.1016/j.nanoen.2020.105555>

- [57] de Fazio, R., Cafagna, D., Marcuccio, G., Minerba, A., & Visconti, P. (2020). A Multi-Source Harvesting System Applied to Sensor-Based Smart Garments for Monitoring Workers' Bio-Physical Parameters in Harsh Environments. *Energies*, 13(9), 2161. <https://doi.org/10.3390/en13092161>
- [58] Chen, L., Xu, X., Zeng, P., & Ma, J. (2014). Integration of Energy Harvester for Self-Powered Wireless Sensor Network Nodes. *International Journal of Distributed Sensor Networks*. 10(4). 782710. <https://doi.org/10.1155/2014/782710>
- [59] Ambient Energy Harvesting Chips for IoT End Devices: Review. (n.d.). Ieexplore.ieee.org. Retrieved September 30, 2023, from <https://ieeexplore.ieee.org/abstract/document/9691438>
- [60] Why voltage multiplier decreases current? (n.d.). Electrical Engineering Stack Exchange. Retrieved October 7, 2023, from <https://electronics.stackexchange.com/questions/542880/why-voltage-multiplier-decreases-current>
- [61] Chouhan, S. S., Nurmi, M., & Halonen, K. (2016). Efficiency enhanced voltage multiplier circuit for RF energy harvesting. *Microelectronics Journal*, 48, 95–102. <https://doi.org/10.1016/j.mejo.2015.11.012>

# APPENDICES

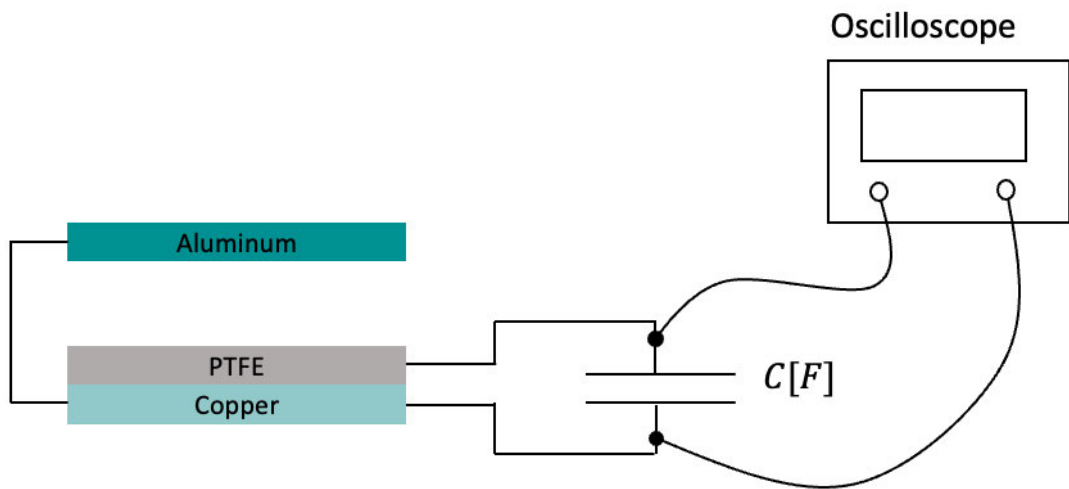
## Appendix A: Equipment Specifications.

Equipment used in this study are as follows:

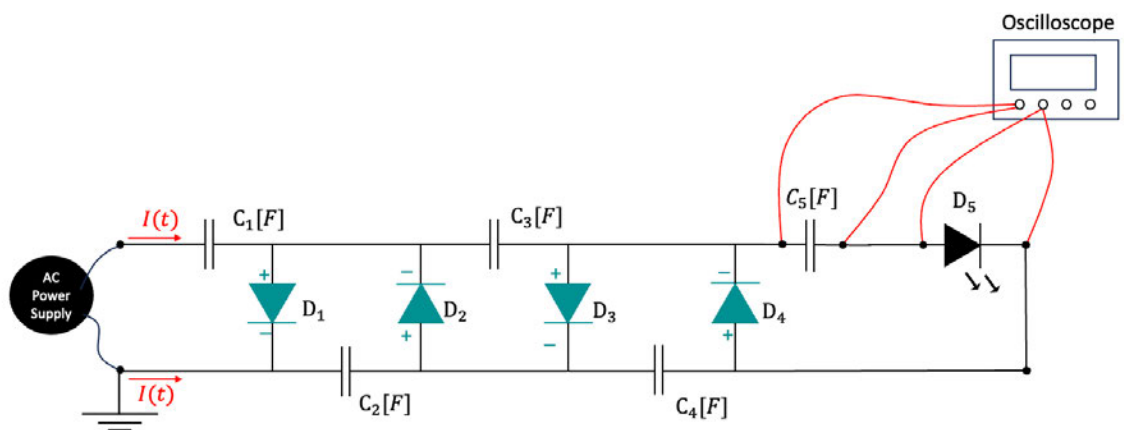
1. Mixed Signal Oscilloscope
  - a. Model: Keysight InfiniiVision MSO-X 2004A
  - b. Manufacturer: Keysight Technologies
  - c. Purpose: Used for precise signal measurement and waveform analysis. Capture and analyse analogue and digital signals, contributing to data acquisition process.
  - d. Specifications:
    - i. Bandwidth: 70MHz
    - ii. Sampling Rate: 2GSa/s
    - iii. Analog Channels: 4
    - iv. Display: 8.5-inch colour TFT LCB with 800x480 pixels.
  - e. Probes: Utilised standard 10:1 passive voltage probe for signal measurements.
  - f. Operating Conditions: Operated within a temperature range of 20° to 25°.
  - g. Data Transfer: Supported USB connectivity for data collection.
2. Triple Output DC Power Supply
  - a. Model: U8031
  - b. Manufacturer: Keysight Technologies
  - c. Purpose: Provide precise and regulated power to various to the LTC3588 energy harvester chip in the experimental set. Controlled voltage levels for data acquisition.
  - d. Specifications:
    - i. Voltage Outputs: Three channels with adjustable ranges but only was used:
      1. Channel 1 & 2: 0-30V range.
      2. Channel 3: 5V
    - ii. Current Outputs:
      1. 6A for 0-30V Channels
      2. 3A for 5V Channel
    - iii. Display: 4-digit LED display for voltage and current readings.
    - iv. Operating Bandwidth: 20 Hz to 20 Mhz.

- e. Control and Interface: DC power supply was controlled using front-panel knobs and digital interface for precise adjustments and monitoring.
  - f. Operating Conditions: Operated within a temperature range of 20° to 25°.
  - g. Connectivity and Outputs: Equipped with banana jacks for easy and secure connections.
3. Dual Display Multi-meter
- a. Model: U3401A
  - b. Manufacturer: Keysight Technologies
  - c. Purpose: Utilised to measure resistor's resistance.
  - d. Specifications:
    - i. Display: Dual Display with 4 ½ digits.
    - ii. Measurement Functions: Voltage (AC/DC), Current (AC/DC), Resistance, Capacitance, Frequency, etc.
  - e. Control and interface: Controlled via front-panel buttons and a digital interface for precise measurements and data logging.
  - f. Operating Conditions: Operated within a temperature range of 20° to 25°.
  - g. Connectivity and Outputs: Equipped with standard banana jacks for secure connections.
4. Series Waveform Generator
- a. Model: 33500B Series
  - b. Manufacturer: Keysight Technologies
  - c. Purpose: Used to produce controlled waveforms.
  - d. Specifications:
    - i. Frequency: 2.5 Hz
    - ii. Waveform Type: Sinusoidal Waveform
    - iii. Amplitude: 4Vpp
    - iv. Output Impedance: High Z
    - v. Display: 4.3-inch colour touch screen for waveform visualisation.
  - e. Control and interface: Controlled via front panel for precise waveform configuration.
  - f. Operating Conditions: Operated within a temperature range of 20° to 25°.

## Appendix B. TENG Configuration

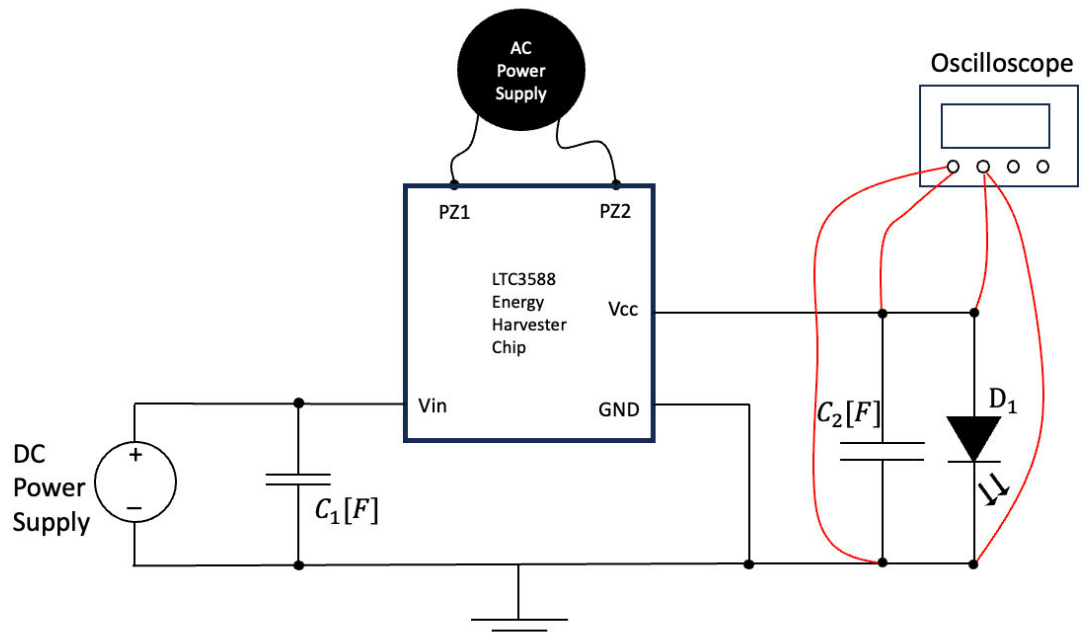


## Appendix C. Voltage Multiplier Circuit Configuration

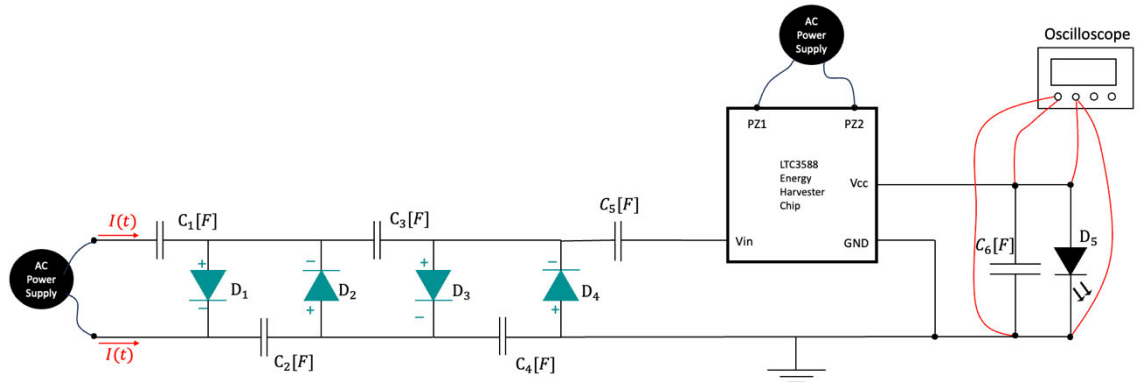




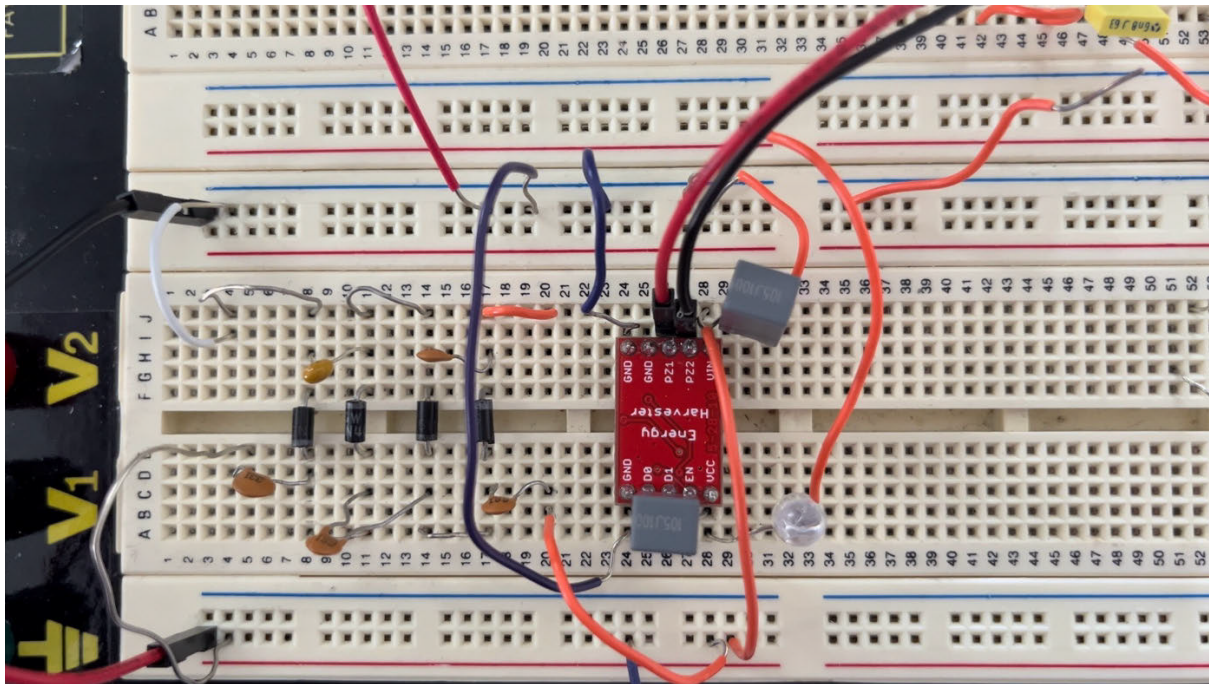
## Appendix D. LTC3588 Energy Harvester Chip Configuration



## Appendix E. Power Management System Configuration



## Appendix F. Power Management System Circuit Design



## Appendix G. Python Code

```
import numpy as np
import matplotlib.pyplot as plt
import pandas as pd
import scipy

# only teng with capacitor - baseline for comparison (need to get one for 1uF)

### --- voltage multiplier circuit only --- ###

# -- TENG with 680pF Capacitor

teng_data = pd.read_csv('TENG_output.csv')
column_name = 'voltage'
teng_680pF = teng_data[column_name]

# -- TENG with 1uF Capacitor
teng_data_1uF = pd.read_csv('1test1.csv')
column_name_2 = 'Voltage'
teng_1uF = teng_data_1uF[column_name_2]

# -- Ideal Input to VMC
VMC_data = pd.read_csv('pms2.csv')
column_name_3 = 'Ideal'
ideal_VMC_data = VMC_data[column_name_3]

# -- TENG input to VMC

teng_VMC_data = pd.read_csv('TENG_VMC.csv')
column_name_4 = 'voltage'
teng_VMC = teng_VMC_data[column_name_4]

### --- ltc chip + voltage mutliplier circui ----- ##

#-- Ideal LTC3588 Energy Harvester Chip
ltc_chip_ideal = pd.read_csv('ltc1ufcap.csv')
column_name_5 = 'Capacitor'
ltc_chip_ideal_capacitor = ltc_chip_ideal[column_name_5]

# -- Ideal Inputs to LTC energy harvester chip and VMC
ideal_ltc_vmc = pd.read_csv('1test3.csv')
column_name_6 = 'Capacitor'
ltc_vmc_ideal = ideal_ltc_vmc[column_name_6]

# -- Ideal DC input (at VMC) to LTC with TENG input at PZ1 and PZ2
ltc_ideal_vmc_teng_at_PZ1_PZ2 = pd.read_csv('1test4.csv')
column_name_7 = 'Capacitor'
ideal_vmc_teng_at_PZ1_PZ2_ltc = ltc_ideal_vmc_teng_at_PZ1_PZ2[column_name_7]

# -- Ideal AC input at PZ1 and PZ2 with TENG input at VMC to DC input of LTC
ideal_ltc_PZ1_PZ2_teng_vmc = pd.read_csv('1test2.csv')
column_name_8 = 'Output Capacitor'
ideal_PZ1_PZ2_ltc_teng_vmc = ideal_ltc_PZ1_PZ2_teng_vmc[column_name_8]

# -- Two TENG input with VMC and LTC Chip
two_teng = pd.read_csv('teng2pms680nfltc7.csv')
column_name_9 = 'Output Cap'
two_teng_outputCap = two_teng[column_name_9]
```

```

## ----- current data ----- ###
# -- ltc chip only with ideal input
current_ideal_chip = pd.read_csv('ideal1komres.csv')
column_name_10 = 'current (rms)'
ideal_current_ltc = current_ideal_chip[column_name_10]

## -- TENG only with Resistor

current_teng = pd.read_csv('teng1kohm.csv')
column_name_11 = 'current (rms)'
current_teng_1kohm = current_teng[column_name_11]

## -- ltc chip + vmc with ideal inputs

current_ideal_chip_vmc = pd.read_csv('pmschipideal1kohm.csv')
column_name_12 = 'current (rms)'
ideal_current_ltc_vmc = current_ideal_chip_vmc[column_name_12]

## -- ltc chip + vmc with AC ideal input (PZ1/PZ2) and TENG input at VMC

current_chip_vmc = pd.read_csv('pmschiptenqd1kohm1.csv')
column_name_13 = 'current (rms)'
current_chip_ACideal_teng_at_vmc = current_chip_vmc[column_name_13]

## -- ltc chip + vmc with DC ideal and TENG input at PZ1/PZ2

current_teng_PZ1_PZ2_ideal_vmc = pd.read_csv('1test5.csv')
column_name_14 = 'current (rms)'
teng_PZ1_PZ2_ideal_vmc_current = current_teng_PZ1_PZ2_ideal_vmc[column_name_14]

## -- ltc chip + vmc with two TENG inputs

current_two_teng = pd.read_csv('test3.csv')
column_name_15 = 'current (rms)'
current_two_teng_output = current_two_teng[column_name_15]

## ----- POWER DATA (based on current excel spreadsheets) ----- ###

# -- ltc chip only with ideal input
power_ideal_chip = pd.read_csv('ideal1komres.csv')
column_name_16 = 'power'
ideal_power_ltc = power_ideal_chip[column_name_16]

## -- TENG only with Resistor

power_teng = pd.read_csv('teng1kohm.csv')
column_name_17 = 'Power'
power_teng_1kohm = power_teng[column_name_17]

## -- ltc chip + vmc with ideal inputs

power_ideal_chip_vmc = pd.read_csv('pmschipideal1kohm.csv')
column_name_18 = 'power'
ideal_power_ltc_vmc = power_ideal_chip_vmc[column_name_18]

## -- ltc chip + vmc with AC ideal input (PZ1/PZ2) and TENG input at VMC

power_chip_vmc = pd.read_csv('pmschiptenqd1kohm1.csv')
column_name_19 = 'power'
power_chip_ACideal_teng_at_vmc = power_chip_vmc[column_name_19]

```

```

## -- ltc chip + vmc with DC ideal and TENG input at PZ1/PZ2

power_teng_PZ1_PZ2_ideal_vmc = pd.read_csv('1test5.csv')
column_name_20 = 'power'
teng_PZ1_PZ2_ideal_vmc_power = power_teng_PZ1_PZ2_ideal_vmc[column_name_20]

## -- ltc chip + vmc with two TENG inputs

power_two_teng = pd.read_csv('test3.csv')
column_name_21 = 'power'
power_two_teng_output = power_two_teng[column_name_21]

## ----- LOW PASS FILTER ----- ##

fs = 30
cutoff = 2
order = 2

def butter_lowpass_filter(data, cutoff, fs, order):

    nyq = 0.5 * fs
    normal_cutoff = cutoff / nyq

    #get filter coefficients
    b, a = scipy.signal.butter(order, normal_cutoff, btype='low', analog=False)
    y = scipy.signal.filtfilt(b, a, data)
    return y

### ----- voltage multiplier circuit only ----- ###

# -- TENG with 680pF Capacitor

filtered_teng_data = butter_lowpass_filter(teng_680pF, cutoff, fs, order)

# -- Ideal Input to VMC

filtered_ideal_VMC_data = butter_lowpass_filter(ideal_VMC_data, cutoff, fs, order)

# -- TENG input to VMC
filtered_teng_VMC = butter_lowpass_filter(teng_VMC, cutoff, fs, order)

### ----- ltc chip + voltage mutliplier circui ----- ##

## -- TENG with 1uF
filtered_teng_1uF = butter_lowpass_filter(teng_1uF, cutoff, fs, order)

##-- Ideal LTC3588 Energy Harvester Chip
filtered_ltc_chip_ideal_capacitor = butter_lowpass_filter(ltc_chip_ideal_capacitor, cutoff, fs, order)

# -- Ideal Inputs to LTC energy harvester chip and VMC
filtered_ltc_vmc_ideal = butter_lowpass_filter(ltc_vmc_ideal, cutoff, fs, order)

# -- Ideal DC input (at VMC) to LTC with TENG input at PZ1 and PZ2
filtered_ideal_vmc_teng_at_PZ1_PZ2_ltc = butter_lowpass_filter(ideal_vmc_teng_at_PZ1_PZ2_ltc, cutoff, fs,
order)

# -- Ideal AC input at PZ1 and PZ2 with TENG input at VMC to DC input of LTC
filtered_ideal_PZ1_PZ2_ltc_teng_vmc = butter_lowpass_filter(ideal_PZ1_PZ2_ltc_teng_vmc, cutoff, fs, order)

```

```

# -- Two TENG input with VMC and LTC Chip

filtered_two_teng_outputCap = butter_lowpass_filter(two_teng_outputCap, cutoff, fs, order)

## ----- current filtered signals ----- ###

filtered_ideal_current_ltc = butter_lowpass_filter(ideal_current_ltc, cutoff, fs, order)

## -- TENG only with Resistor

filtered_current_teng_1kohm = butter_lowpass_filter(current_teng_1kohm, cutoff, fs, order)

## -- ltc chip + vmc with ideal inputs

filtered_ideal_current_ltc_vmc = butter_lowpass_filter(ideal_current_ltc_vmc , cutoff, fs, order)

## -- ltc chip + vmc with AC ideal input (PZ1/PZ2) and TENG input at VMC

filtered_current_chip_ACideal_teng_at_vmc = butter_lowpass_filter(current_chip_ACideal_teng_at_vmc,
cutoff, fs, order)
## -- ltc chip + vmc with DC ideal and TENG input at PZ1/PZ2

filtered_teng_PZ1_PZ2_ideal_vmc_current = butter_lowpass_filter(teng_PZ1_PZ2_ideal_vmc_current, cutoff,
fs, order)

## -- ltc chip + vmc with two TENG inputs
filtered_current_two_teng_output = butter_lowpass_filter(current_two_teng_output, cutoff, fs, order)

##### ----- Power filtered signals ----- #####

filtered_ideal_power_ltc = butter_lowpass_filter(ideal_power_ltc, cutoff, fs, order)

## -- TENG only with Resistor

filtered_power_teng_1kohm = butter_lowpass_filter(power_teng_1kohm, cutoff, fs, order)

## -- ltc chip + vmc with ideal inputs

filtered_ideal_power_ltc_vmc = butter_lowpass_filter(ideal_power_ltc_vmc , cutoff, fs, order)

## -- ltc chip + vmc with AC ideal input (PZ1/PZ2) and TENG input at VMC

filtered_power_chip_ACideal_teng_at_vmc = butter_lowpass_filter(power_chip_ACideal_teng_at_vmc, cutoff,
fs, order)
## -- ltc chip + vmc with DC ideal and TENG input at PZ1/PZ2

filtered_teng_PZ1_PZ2_ideal_vmc_power = butter_lowpass_filter(teng_PZ1_PZ2_ideal_vmc_power, cutoff, fs,
order)

## -- ltc chip + vmc with two TENG inputs
filtered_power_two_teng_output = butter_lowpass_filter(power_two_teng_output, cutoff, fs, order)

## ----- plotting voltage multiplier ----- ##

#teng testing for voltage multiplier
plt.figure(1)

# -- TENG with 680pF Capacitor

plt.plot(filtered_teng_data, label='TENG', linestyle='-', color='blue')

```

```

# -- Ideal Input to VMC
#plt.plot(filtered_ideal_VMC_data, label='ideal_VMC_data', linestyle='-', color='green')
# -- TENG input to VMC
plt.plot(filtered_teng_VMC, label='TENG Input to VMC', linestyle='-', color='red')

## ----- plotting LTC and Voltage Multipler ----- ##
plt.figure(2)

## -- TENG with 1uF Cap

plt.plot(filtered_teng_1uF, label='TENG with 1uF', linestyle='-', color='blue')

#-- Ideal LTC3588 Energy Harvester Chip
plt.plot(filtered_ltc_chip_ideal_capacitor, label='Ideal Input to LTC3588', linestyle='-', color='black')

# -- Ideal Inputs to LTC energy harvester chip and VMC
plt.plot(filtered_ltc_vmc_ideal, label='Ideal Input to Power Management System', linestyle='-', color='green')

# -- Ideal DC input (at VMC) to LTC with TENG input at PZ1 and PZ2
plt.plot(filtered_ideal_vmc_teng_at_PZ1_PZ2_ltc, label='Ideal Input VMC and TENG Input to LTC3588',
linestyle='-', color='purple')

# -- Ideal AC input at PZ1 and PZ2 with TENG input at VMC to DC input of LTC
plt.plot(filtered_ideal_PZ1_PZ2_ltc_teng_vmc, label='Ideal Input to LTC3588 and TENG Input to VMC',
linestyle='-', color='red')

# -- Two TENG input with VMC and LTC Chip
plt.plot(filtered_two_teng_outputCap, label='Two TENG Input to VMC and LTC3588', linestyle='-',
color='orange')

# Add title and labels
plt.title('Voltage Data of Power Management System')
plt.xlabel('Time [s]')
plt.ylabel('Amplitude [V]')
plt.grid(True)

# Add a legend
plt.legend()

# Show the plot
plt.show()

## ---- plotting current ---- #
plt.figure(3)

## ----- current filtered signals ---- ###
plt.plot(filtered_ideal_current_ltc, label='Ideal Input to LTC3588', linestyle='-', color='blue')

## -- TENG only with Resistor
plt.plot(filtered_current_teng_1kohm, label='Ideal Input to LTC3588 and TENG Input to VMC', linestyle='-',
color='red')

## -- ltc chip + vmc with ideal inputs
plt.plot(filtered_ideal_current_ltc_vmc, label='Ideal Input to Power Management System', linestyle='-',
color='green')

## -- ltc chip + vmc with AC ideal input (PZ1/PZ2) and TENG input at VMC
plt.plot(filtered_current_chip_ACideal_teng_at_vmc, label='TENG 60mm Diameter', linestyle='-',
color='purple')

```

```

## -- ltc chip + vmc with DC ideal and TENG input at PZ1/PZ2
plt.plot(filtered_teng_PZ1_PZ2_ideal_vmc_current, label='Ideal Input to VMC and TENG Input to LTC3588',
linestyle='-', color='pink')

## -- ltc chip + vmc with two TENG inputs
plt.plot(filtered_current_two_teng_output, label='Two TENG Inputs Only', linestyle='-', color='orange')

# Add title and labels
plt.title('Current Data')
plt.xlabel('Time[s]')
plt.ylabel('Amplitude [A]')
plt.grid(True)

# Add a legend
plt.legend()

# Show the plot
plt.show()

##### ----- plotting power values ----- #####
plt.figure(4)

## ----- current filtered signals ---- ###
plt.plot(filtered_ideal_power_ltc, label='Ideal Input to LTC3588', linestyle='-', color='blue')

## -- TENG only with Resistor
plt.plot(filtered_power_teng_1kohm, label='Ideal Input to LTC3588 and TENG Input to VMC', linestyle='-',
color='red')

## -- ltc chip + vmc with ideal inputs
plt.plot(filtered_ideal_power_ltc_vmc, label='Ideal Input to Power Managment System', linestyle='-',
color='green')

## -- ltc chip + vmc with AC ideal input (PZ1/PZ2) and TENG input at VMC
plt.plot(filtered_power_chip_ACideal_teng_at_vmc, label='TENG 60mm Diameter', linestyle='-', color='purple')

## -- ltc chip + vmc with DC ideal and TENG input at PZ1/PZ2
plt.plot(filtered_teng_PZ1_PZ2_ideal_vmc_power, label='Ideal Input to VMC and TENG Input to LTC3588',
linestyle='-', color='pink')

## -- ltc chip + vmc with two TENG inputs
plt.plot(filtered_power_two_teng_output, label='Two TENG Inputs Only', linestyle='-', color='orange')

# Add title and labels
plt.title('Power Data')
plt.xlabel('Time[s]')
plt.ylabel('Watts [W]')
plt.grid(True)

# Add a legend
plt.legend()

# Show the plot
plt.show()

```



## Appendix H. Python Code for Statistical Analysis

### Voltage Data from Power Management System

```
import pandas as pd
import numpy as np
import matplotlib.pyplot as plt
from scipy.signal import butter, filtfilt

# Create an empty list to store the voltage data from each file
voltage_data = []

# Create empty lists to store the filtered data and statistics for each 'voltage' data set
filtered_data = []
error_percentages = []
std_deviations = []
percentiles_95 = []
means = []

# Define the Butterworth filter parameters
fs = 30 # Assuming a sampling rate of 1000 Hz
cutoff_frequency = 2 # Cutoff frequency in Hz
order = 2 # Filter order

# Design the Butterworth filter
nyquist = 0.5 * fs
normal_cutoff = cutoff_frequency / nyquist
b, a = butter(order, normal_cutoff, btype='low', analog=False)

# Loop through the 10 Excel files (scope_0 to scope_9)
for i in range(10, 20):
    file_name = f'scope_{i}.csv' # Replace with the actual file extension if needed
    df = pd.read_csv(file_name) # Read the Excel file into a DataFrame
    voltage_column = df['voltage'] # Extract the 'voltage' column

    # Apply the Butterworth filter to the 'voltage' data
    filtered_voltage = filtfilt(b, a, voltage_column)
    filtered_data.append(filtered_voltage)

    # Calculate standard deviation, 95th percentile, and mean
    std_deviations.append(filtered_voltage.std())
    percentiles_95.append(np.percentile(filtered_voltage, 95))

    # Calculate mean using only positive values
    positive_mean = np.mean(filtered_voltage[filtered_voltage > 0])
    means.append(positive_mean)

    # Store the voltage data for later use
    voltage_data.append(filtered_voltage)

# Calculate the average of each 'voltage' data set using only positive values
positive_averages = [np.mean(voltage[voltage > 0]) for voltage in voltage_data]

# Calculate error percentage between the averages of each data set
for i in range(1, 10):
    error_percentage = ((positive_averages[i] - positive_averages[0]) / positive_averages[0]) * 100
    error_percentages.append(error_percentage)

# Create a bar graph for Error Percentage Between Averages
plt.figure(figsize=(8, 6))
```

```

plt.bar(range(1, 10), error_percentages, tick_label=[f'scope_{i}' for i in range(1, 10)])
plt.title('Error Percentage Between Averages (Using Positive Values)')
plt.xlabel('Data Set')
plt.ylabel('Error Percentage')

plt.show()

# Plot the 95th Percentile
plt.figure(figsize=(8, 6))
plt.bar(range(10), percentiles_95, tick_label=[f'scope_{i}' for i in range(10)])
plt.title('95th Percentile of Voltage Data from Power Management System')
plt.xlabel('Data Set')
plt.ylabel('95th Percentile')

plt.show()

# Plot the Standard Deviation
plt.figure(figsize=(8, 6))
plt.bar(range(10), std_deviations, tick_label=[f'scope_{i}' for i in range(10)])
plt.title('Standard Deviation of Voltage Data from Power Management System')
plt.xlabel('Data Set')
plt.ylabel('Std Deviation')

plt.show()

# Create a single figure with subplots for all three plots
fig, axs = plt.subplots(1, 2, figsize=(12, 6))

# Plot the 95th Percentile
axs[0].bar(range(10), percentiles_95, tick_label=[f'scope_{i}' for i in range(10)], color='purple')
axs[0].set_title('95th Percentile of Voltage Data from Voltage Multiplier Circuit')
axs[0].set_xlabel('Data Set')
axs[0].set_ylabel('95th Percentile')

# Plot the Standard Deviation
axs[1].bar(range(10), std_deviations, tick_label=[f'scope_{i}' for i in range(10)])
axs[1].set_title('Standard Deviation of Voltage Data from Voltage Multiplier Circuit')
axs[1].set_xlabel('Data Set')
axs[1].set_ylabel('Std Deviation')

plt.tight_layout() # Adjust spacing between subplots
plt.show()

```

## Current Data from Power Management System

```
import pandas as pd
import numpy as np
import matplotlib.pyplot as plt
from scipy.signal import butter, filtfilt

# Create empty lists to store the statistics for each 'current(rms)' data set
std_deviations = []
percentiles_95 = []

# Define the Butterworth filter parameters
fs = 30 # Sampling frequency
cutoff_frequency = 2 # Cutoff frequency in Hz
order = 2 # Filter order

# Design the Butterworth filter
nyquist = 0.5 * fs
normal_cutoff = cutoff_frequency / nyquist
b, a = butter(order, normal_cutoff, btype='low', analog=False)

# Create subplots
fig, axes = plt.subplots(1, 2, figsize=(8, 10))

# Loop through the 10 Excel files (scope_20.csv to scope_29.csv)
for i in range(20, 30):
    file_name = f'scope_{i}.csv' # Construct the file name
    try:
        df = pd.read_csv(file_name) # Read the CSV file into a DataFrame
        current_column = df['current(rms)'] # Extract the 'current(rms)' column

        # Apply the Butterworth filter to the 'current(rms)' data
        filtered_current = filtfilt(b, a, current_column)

        # Calculate standard deviation
        std_deviation = np.std(filtered_current)
        std_deviations.append(std_deviation)

        # Calculate 95th percentile
        percentile_95 = np.percentile(filtered_current, 95)
        percentiles_95.append(percentile_95)
    except FileNotFoundError:
        print(f'File '{file_name}' not found.')

# Plot the 95th Percentile
axes[0].bar(range(10), percentiles_95, tick_label=[f'scope_{i}' for i in range(20, 30)], color='purple')
axes[0].set_title('95th Percentile of Current Data of Power Management System')
axes[0].set_xlabel('Data Set')
axes[0].set_ylabel('95th Percentile')

# Plot the Standard Deviation
axes[1].bar(range(10), std_deviations, tick_label=[f'scope_{i}' for i in range(20, 30)])
axes[1].set_title('Standard Deviation of Current Data of Power Management System')
axes[1].set_xlabel('Data Set')
axes[1].set_ylabel('Std Deviation')

plt.tight_layout() # Adjust spacing between subplots
plt.show()
```